Microwave multiphoton ionization and excitation of helium Rydberg atoms

Willem van de Water
Physics Department, Eindhoven University of Technology, P.O. Box 513, 5600 MB Eindhoven, The Netherlands

Suzanne Yoakum
Department of Physics, State University of New York at Stony Brook, Stony Brook, New York 11794

Ton van Leeuwen
Physics Department, Eindhoven University of Technology, P.O. Box 513, 5600 MB Eindhoven, The Netherlands

Ben E. Sauer and Leo Moorman
Department of Physics, State University of New York at Stony Brook, Stony Brook, New York 11794

Enrique J. Galvez
Department of Physics and Astronomy, Colgate University, Hamilton, New York 13346

David R. Mariani
Schlumberger-Doll Research, Ridgefield, Connecticut 06877

Peter M. Koch
Department of Physics, State University of New York at Stony Brook, Stony Brook, New York 11794
(Received 16 October 1989; revised manuscript received 16 April 1990)

We study experimentally and theoretically the detailed field-amplitude dependence of the multiphoton ionization and excitation probability of highly excited $n_0\,^3S$ helium atoms in a 9.924-GHz linearly polarized microwave electric field. For ionization, with principal quantum numbers in the range $n_0=25-32$, we use a quasistatic analysis that employs integration of the time-dependent Schrödinger equation using basis states of the static field Hamiltonian. The calculated results are used to interpret the observed ionization threshold structure. For excitation, the results of $n_0\,^3S\rightarrow n_0\,^3L$, $L>2$ excitation experiments are explained quantitatively and precisely using a theory of multiphoton resonances. We present maps of quasienergy levels that allow the study of the dynamics of the field-switching transients. These transient effects are analyzed along the lines of standard atomic collision theory and are shown to determine the shape of the observed resonances.

I. INTRODUCTION

The behavior of atoms or molecules in intense electromagnetic fields is of an intriguing complexity. Intense in this context roughly means that multiphoton transitions of high order, maybe even into the continuum, are driven with non-negligible probability. Multiphoton transitions between bound states would become important when the interaction energies associated with electric dipole matrix elements become comparable to the level splitting. We also expect the possibility of multiphoton ionization to come into play when the electric amplitude of the radiation field becomes non-negligible compared to the strength of the Coulomb field binding the valence electron. Of course, these are very crude notions that bypass many essential subtleties associated with the presence of resonances between real or virtual states of the atom-field system.

The experimental challenge is to produce sources of electromagnetic radiation that are intense in the above sense. For tightly bound atoms or molecules, this has been accomplished only with pulsed lasers. Though these are now widely available, such lasers whose radiation fields have spatio-temporal profiles that are characterized and stable from shot to shot are less common. There has been an inexorable drive towards ever shorter laser pulses, now even less than 100 fs.

Another way to meet this experimental challenge is to use atoms with a very weakly bound valence electron, i.e., Rydberg atoms. Because of the large interaction matrix elements, small energy splittings, and weak Coulomb binding fields, it is quite straightforward to access the intense field regime with a continuous microwave field whose strength in laboratory units is quite modest. Through selection of the principal quantum number n_0 of the initial state, the response to fields generated by standard microwave equipment (with frequency $\omega/2\pi$ ranging from 1 to 36 GHz) ranges from quasistatic for $n_0\cong 20$ at several GHz, to strongly resonant for $n_0\cong 90$ in a 10-GHz field, where the frequency of the microwave oscillations is approximately in tune with the unperturbed electronic orbital frequency (n_0^{-3}, atomic units are used throughout). The high-frequency regime, where a single photon energy suffices to bridge locally nearly three n

values, is entered with atoms of $n_0 \cong 70$ in a 36-GHz field.

The latter regime is nowadays subject of lively research. Especially for hydrogen atoms it has come to be a testing ground for investigations of quantal dynamics in systems whose classical counterparts exhibit a transition to chaos.[1] The present article focuses on the first, low-frequency regime, for which we will discuss ionization and excitation experiments of helium $(1sn_0s)^3S$ Rydberg atoms prepared in states with $n_0 = 25-32$ in a fast-beam apparatus. A recent paper, whose author list included some of us, focused on low- (scaled) frequency microwave ionization behavior of highly excited hydrogen atoms.[2] A noteworthy similarity between the results in this paper (with scaled frequency $n_0^3\omega < 0.05$) and the hydrogen results ($n_0^3\omega \lesssim 0.2$) is the not uncommon presence of (sharp) structures in the microwave ionization curves. Although classical dynamics can explain many aspects of the microwave ionization of hydrogen Rydberg atoms, those structures are of quantal origin. Classically, the scaled frequency $n_0^3\omega$ is the ratio of ω and the mean Kepler frequency for the hydrogen atom with initial principal action $I_0 = n_0\hbar$. Quantally, the inverse of $n_0^3\omega$ is also approximately the number of photons needed to bridge adjacent (hydrogenic) n_0 manifolds.

As is well known, in nonhydrogenic atoms the interaction of the excited electron with the atomic core destroys the dynamical symmetry that characterizes the response of hydrogen atoms to an electric field.[3] This is reflected in the energy spectrum as a function of static field strength which possesses ubiquitous anticrossings. In the quasistatic view, nonadiabatic behavior in a changing electric field is concentrated near those anticrossings. Pillet *et al.*[4] and Mariani *et al.*[5] showed that the ionization threshold field amplitude in an oscillating field is much lower than the threshold in a static electric field. The threshold field amplitude was shown to scale with the principal quantum number as $F_{\text{thr}} \simeq n_0^{-5}$, which is also the scaling of the static field strength were states of the n_0 manifold first avoid crossing with those of its neighboring $n_0 - 1$ and $n_0 + 1$ manifolds.[4]

In the present article we will concentrate on the detailed ionization behavior as a function of microwave electric-field amplitude of $\text{He}(1sn_0s)^3S_1$ Rydberg atoms for a few n_0 values. In view of the above we will primarily seek an explicit time-dependent description of the atomic response to the instantaneous electric field. Such a description emphasizes the role of anticrossings between levels in a static electric field. It will turn out that already for the principal quantum numbers of interest ($n_0 \cong 30$) this idea is hardly adequate: The rate of change of the instantaneous field is almost always so large that nonadiabatic effects do not remain confined to isolated values of the electric-field strength where anticrossings occur.

The time-dependent Hamiltonian that describes the response of an atom to a harmonic excitation may be transformed into a time-independent one by Floquet analysis. Although the results of such an analysis are identical to those of an explicit time-dependent approach, it emphasizes the photon character of the interaction with the radiation field. The eigenstates and eigenenergies (quasienergies) that constitute the spectrum of the Floquet Hamiltonian may in the semiclassical limit be interpreted as atom-field states and energies. In case of the excitation experiments, where such an analysis turns out to be affordable, this circumstance will enable us to concentrate on the remaining slow time dependence, namely that of the switching transients of the radiation field. The importance of understanding these transients may be appreciated by realizing that a radiation field, even a very strong one, that is turned on slowly enough, and again turned off slowly enough, would leave the atom in its initial state. Slow in this context means slow with respect to the inverse width of all anticrossings between atom-field states that are traversed when the field amplitude is increased to its maximum and back again to zero.

Floquet analysis thus provides a crucial refinement of the concepts outlined above: Nonadiabatic effects are concentrated at anticrossings between *quasi-energy* states. The anticrossings between atomic levels in a *static* electric field provide only very coarse guidance as to which Floquet anticrossings between levels based on neighboring manifolds n and $n+1$ will be sizable.

The separation of fast and slow time scales is a well-known concept in the theory of atomic collisions.[6] When the motion of the nuclei is slow with respect to the electronic motion, the collision system can be thought of as evolving on potential surfaces that arise from the almost immediate adjustment of the electronic configuration to the changing internuclear separation. In the present context, much as in collision physics, the atomic response to the switching transient of a radiation field can be viewed as the almost immediate adjustment of the quasienergy spectrum to the slowly varying field amplitude. Quasienergy levels then will play the same role as do potential-energy surfaces in collision physics.

The importance of controlling the shape of the radiation pulse has long been recognized in radio-frequency spectroscopy.[7] The analogy between the physics of strong radiation fields and the physics of atomic collisions has been recognized by Breuer, Dietz, and Holthaus, who correlated the explicit time dependence of a model system with the properties of its quasienergy spectrum.[8] A calculational scheme for the study of transient effects, much along the lines laid out in the present paper, has been proposed previously by Szöke.[9] In the past few years strong laser sources with very short pulse lengths have become widely available, and understanding the effects of the pulse shape appears to be a very timely problem.[10] For example, 100-fs laser pulses with a wavelength centered at 620 nm have been used in multiphoton ionization and so-called "above-threshold ionization" experiments with strongly bound atoms. In such laser pulses the optical field oscillates only about 50 times. This is comparable to the approximately 500 oscillations in the microwave pulses in the present paper.

Although the existence of two time scales in the interaction between pulses of strong radiation and matter may be intuitively clear, it is not at all obvious whether this concept will lead to practical calculational schemes in circumstances of physical relevance. We feel that the system described in this paper provides an ideal testing

ground for showing the utility of these ideas.

In the experiments discussed in this paper the switch-on and switch-off of the longitudinally directed oscillating electric field takes place in the rest frame of the atoms that fly through a microwave cavity. The switch-on occurs in the microwave fringe field extending outwards from the cavity entrance hole, whereas the converse happens in the fringe field extending from the exit hole. By changing these fringe fields (and/or the beam velocity) a very precise control over the switching of the field as experienced by the moving atoms could be realized. Comparable control is very hard to achieve in pulsed laser experiments, where the pulse shape may vary appreciably from shot to shot. At the same time we shall demonstrate that for the intra-n_0-manifold transitions of present experimental interest, the computation of the quasienergy spectrum and associated transition probabilities can be done precisely with only modest computational means.

Section II of this paper describes the experimental techniques used both for ionization and excitation measurements. An important ingredient is the selective detection by field ionization of atoms excited to states of large angular momentum, which is explained in Sec. III. That section also presents the results of our ionization and excitation experiments. Section IV contains an interpretation of both types of experimental results. This interpretation evolves from an explicit time-dependent description in the case of the ionization experiments to a Floquet analysis, supplemented by a time-dependent analysis involving the field *envelope* in the case of the excitation experiments. The formalism used in describing both time dependences is well known, being adapted quite directly from standard atomic collision theory. Appendix A records details about the computation of matrix elements, whereas Appendix B describes tools used for efficient organization of the computation of quasienergy spectra and multiphoton transition probabilities for Rydberg atoms.

Similar microwave amplitude spectra for potassium and barium Rydberg atoms have been obtained by Stoneman and co-workers[11] and Eichmann *et al.*[12] The structure observed in potassium was very broad, the structures observed in barium were narrower, but still significantly less sharp than those reported here for helium. Despite their large variation in width (0.2 in K, 0.04 in He, as normalized on the center field amplitude), we speculate that these structures all have a similar origin. Indeed, a first explanation for the broad feature observed in potassium has been formulated in terms of a Floquet analysis by Stoneman and co-workers.[11,13] We also would like to mention the work of Singh, Sun, and MacAdam, who studied the transient response of Na Rydberg atoms to a weak microwave radiation field.[14] Their work is related to that discussed here, except that in their case the transition is brought into resonance by an external static electric field whereas in the present case resonances are induced by the radiation field itself.

II. EXPERIMENT

Highly excited helium atoms traveling in a fast atomic beam were prepared in $n_0\,{}^3S$, $n_0=25-32$, states by two-step, double-resonance laser excitation in separate regions of static electric field. The electric fields served to Stark-tune the atomic transitions to the (Doppler-shifted) frequency of the laser light which emerged from two separate CO_2 lasers. The $n_0\,{}^3S$ atoms prepared in this way subsequently entered a microwave cavity where they experienced the axial electric field of its TM_{020} mode. Experiments were done with the experimental setup corresponding to two complementary modes: In the first case, or ionization mode, the number of He^+ ions produced inside the cavity was measured as a function of microwave power; in the second, or quench mode, atoms that remained in the initial $n_0\,{}^3S$ state were detected.

A. Preparation of a beam of $n\,{}^3S$ Rydberg atoms

Figure 1 shows the atomic beam arrangement that has been described earlier by some of us.[15] Electron-transfer collisions of 7–17-keV He^+ ions with xenon atoms contained in a gas scattering cell (not shown here) produced a fast beam of excited and ground-state atoms with a kinetic-energy spread $\Delta E/E<0.003$. The beam then traversed the first region of horizontally directed electric

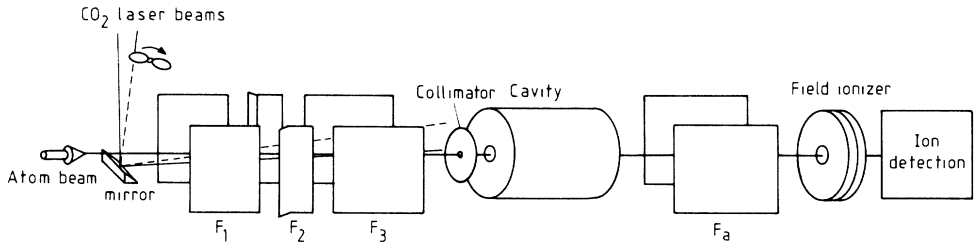

FIG. 1. Schematic drawing of the apparatus. A beam of excited- and ground-state atoms enters from the left and is crossed at shallow angles by two different CO_2 lasers in regions of electric field F_1 and F_3. The electric field F_2 avoids a region of zero field between F_1 and F_3. This double-resonance laser-excitation scheme prepares helium atoms in $n\,{}^3S$ highly excited states. After exposure to $(0.5-1)\times10^3$ oscillations of a 9.924-GHz microwave field, surviving $n\,{}^3S$ atoms are selectively field ionized. The ions are deflected off axis (not shown) and detected by a Johnston particle multiplier. The output signal current is detected in phase with the mechanically chopped F_1 laser beam. The distribution over substates of atoms emerging from the cavity could be analyzed by a separate set of field plates F_a. The collimator preceding the cavity determines the radial extent of the atomic beam.

field F_1 where it was crossed with a $^{12}C^{16}O_2$ laser beam. The infrared radiation excited a fraction of the atoms from one well-defined Stark state in the $n=7$ triplet helium manifold to another one in the $n=9$ or 10 manifold. A second transition with another $^{12}C^{16}O_2$ laser was driven in a region of electric field F_3. The intermediate field region F_2 (strength of 200–400 V/cm) provided for a smooth transition between F_1 and F_3, preserving the state definition between the first and second step of the excitation. The field F_1 (with strength $\cong 20$ kV/cm) also served to deflect remaining ions out of the atomic beam and to ionize atoms with principal quantum numbers $n \gtrsim 11$. The vertical component of the earth's magnetic field along the beam line was canceled with an applied opposing field with a strength of about 0.5 G. The 0.2-G horizontal component was not canceled. In the rest frame of the atoms it produced a vertically directed motional electric field with a strength <0.2 V/cm.

By a judicious choice of the frequencies and linear polarization direction of the two lasers, and of the electric-field strengths F_1 and F_3, beams of $n_0\,^3S$ atoms with principal quantum numbers in the range $n_0=25-32$ could be prepared with a satisfactory intensity (beam currents up to 10^6 s^{-1}). The preparation sequence was guided by a computation of Stark energies and transition probabilities using a matrix diagonalization technique.[16] As one example out of many, we consider the excitation of He atoms to the $29\,^3S$ state via the following sequence:

$$\text{“}7\,^3D(|M_L|=1)\text{”} \rightarrow \text{“}10\,^3P(M_L=0)\text{”} \rightarrow \text{“}29\,^3S(M_L=0)\text{”} ,$$

where the notation in quotation marks designates the zero-field state to which the respective Stark state joins *adiabatically* when $F_{1,3}\rightarrow 0$. The first transition was driven in $F_1=19.806$ kV/cm by photons with $\lambda^{-1}=1081.087$ cm^{-1} (the wave number of the 9μ-$R24$ line of the $^{12}C^{16}O_2$ laser in the lab frame) and polarization perpendicular to the field direction. The second transition was driven in $F_3=42.30$ V/cm by photons with $\lambda^{-1}=980.914$ cm^{-1} ($10\mu-R28$ line) and polarization parallel to the field direction. Both laser beams crossed the atomic beam at small angles (10.7° and 4.2°, respectively). The beam energy was $E_B=11.02$ keV, corresponding to a velocity of 7.29×10^5 m/s, and an associated Doppler shift of the laser light in the rest frame of the atoms of about -0.2% in frequency. The intermediate field F_2 preserved the definition of the intermediate state. A necessary condition is that the Stark shift of the $10\,^3P$ state is larger than its fine-structure splitting, which is the case at the typical setting of F_2 ($\simeq 200$ V/cm).

B. Modes of operation

In the ionization mode, positive ions were born from neutral atoms inside the microwave cavity, which was biased with a label voltage of $V_L=200$ V. These ions, "labeled" at energy E_B+eV_L, were energy selected and detected by a Johnston MM1 particle multiplier that was operated as a linear current amplifier. Its output signal was detected in phase with the mechanically chopped laser interacting in F_1 and was stored in a multichannel analyzer operated in the multiscaling mode. The power incident upon the microwave cavity (and consequently the electric-field amplitude inside) was varied synchronously with the channel advance. By taking a large number of sweeps, slow variations in particle- and laser-beam intensities were averaged out.

In the quench mode, the cavity body was grounded to the rest of the apparatus. Ions produced inside the cavity were not detected; rather Rydberg atoms that emerged from the cavity were ionized in a static longitudinal electric field inside a separate ionizer assembly downstream of the cavity. The voltages on the entrance and exit plates of the ionizer were empirically adjusted such that ions born inside the ionizer were energy labeled in a range of energies that could be detected efficiently. The detection of these ions then proceeded as in the ionization mode. In an almost complementary detection mode, which we will term "unquench mode," atoms formed inside the cavity were ionized in a region of static electric field F_a, immediately following the cavity. The only atoms detected in this mode were those whose static field ionization threshold exceeded the field strength F_a. In Sec. III B 1 of this paper we will show that the unquench technique could be arranged to accept only atoms that were excited by the microwave field to high-L ($L\geq 2$) states with the initial n_0 value.

C. Microwave electric field

A small fraction of the power leaked out of the entrance and exist holes of the cavity, causing a gradual turn-on and turn-off of the field amplitude in the rest frame of the moving atoms. On the beam axis the atoms experienced a field whose time dependence is given by $\mathbf{F}(t)=F_0 A(t)\sin(\omega t+\varphi)\mathbf{e}_z$. They entered the cavity with random phases φ. The distribution of the electric-field amplitude inside and outside the cavity was numerically computed using a finite-element technique.[17] By changing the shape and size of the holes, the shape of the amplitude envelope function $A(t)$ could be controlled. The numerically computed *radial* dependence of the longitudinal electric-field amplitude F_z inside the cavity with radius R was accurately reproduced by

$$F_z(\rho)=F_0 J_0(x_{02}\rho/R) , \tag{1}$$

where F_0 is the value on the beam axis ($\rho=0$). Equation (1) is the analytical result for an ideal cylindrical TM_{020}-mode cavity expressed in terms of a Bessel function J_0 with x_{02} as its second zero. The radial extent of the atomic beam was determined by a collimator that preceded the cavity. In the microwave excitation experiments discussed here, two types of cavities were used: a cavity with tapered entrance and exit holes, causing a gradual turn-on of the microwave field, and a cavity with smaller, untapered, cylindrical apertures that caused a much sharper turnon. Details of those cavities, including the radii of the preceding collimator apertures, are given in entries *II*, *III*, and *IV* of Table I. For both cavities *II* and *IV* we show the numerically computed amplitude en-

TABLE I. List of microwave cavities used. Tapered apertures are represented by two radii, the smallest of which gives the radius of the circle facing the inside of the cavity. The endcap thickness was 0.292 cm, the cavity radius was 2.658 cm. The number of oscillations does not include those in the fringe fields; for cavity *IV* a typical variability across different measurements [see Figs. 8(a) and (b)] is given.

Cavity	Length (cm)	Entrance aperture radius (cm)	Exit aperture radius (cm)	Collimator aperture radius (cm)	Number of microwave oscillations
I	9.870	0.419	0.578	0.251	1100
		0.325	0.321		
II	4.928	0.325	0.321	0.251	550
III	4.928	0.325	0.321	0.602	544
IV	4.928	0.128	0.128	0.044	550(5)

velope function $A(t)$ in Fig. 2.

The cylindrical copper microwave cavities had an inner radius of $R=2.658$ cm and were coupled to a waveguide network by an iris in the sidewall of the cavity. Directional couplers permitted sampling of the power incident on and reflected from the cavity. The microwave power was delivered by a yttrium iron garnet–tuned solid-state oscillator that was followed by a traveling-wave amplifier. The cavity mode (as perturbed by the endcap holes and coupling iris) resonated at $\omega/2\pi=9.924$ GHz with a bandwidth of the order of 1 MHz. The TM_{020} mode consists of an oscillating axial electric field whose amplitude is constant over the length of the cavity and an oscillating azimuthal magnetic field that vanishes on the beam axis. Though atoms off the beam axis experienced a small magnetic field component, its influence was calculated to be completely negligible.

In principle, the on-axis microwave electric field strength F_0 can be determined from a measurement of the power P dissipated in the cavity:

$$F_0=\left[\frac{2PQ_0\omega}{\pi\epsilon_0 LR^2J_1^2(x_{02})}\right]^{1/2}, \tag{2}$$

where Q_0 is the unloaded quality factor of the cavity, ϵ_0 the vacuum permittivity constant, and ω the resonant angular frequency. However, there are many important subtleties involved in a precise measurement of Q_0 and P. Those have been dealt with in a carefully designed procedure that has been described elsewhere.[18] As a result, the field amplitude throughout the part of the cavity traversed by the atoms is known to 5%.

III. RESULTS

A. Ionization experiments

For the ionization experiments atoms were prepared in $n_0\,^3S$ states which subsequently experienced about 1100 oscillations of the electric field in a 9.87-cm-long cavity (cavity *I* in Table I). The experiment then measured the current of ions emerging from the cavity as a function of the electric field amplitude. Figure 3 shows the ioniza-

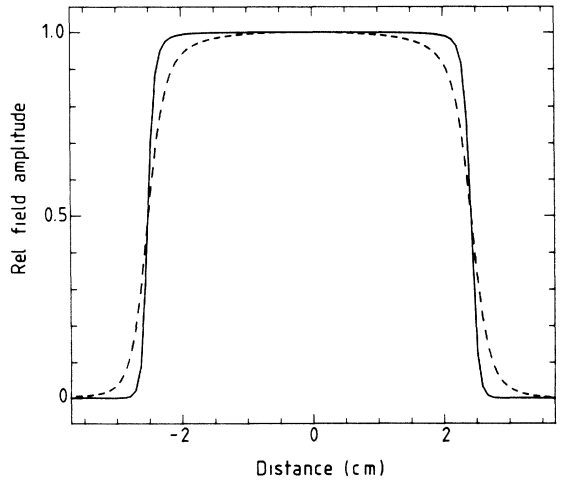

FIG. 2. Electric field amplitude $A(t)$ normalized to the maximum amplitude inside the microwave cavity. On the horizontal scale of the figure, the cavity entrance is located at -2.46 cm and its exit at 2.46 cm. Solid line: fast turn-on in cavity *IV*; dashed line: slower turn-on in cavity *II* (*III*).

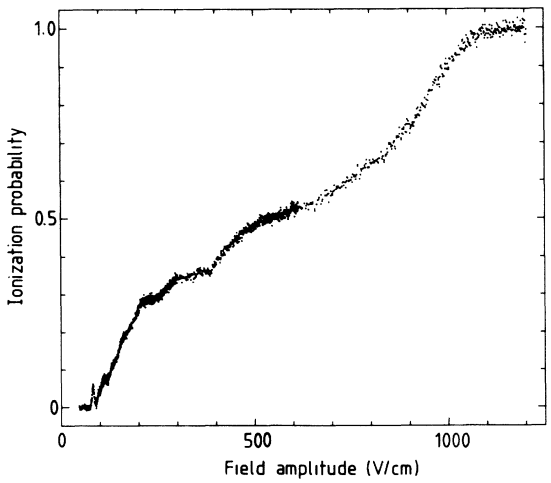

FIG. 3. Microwave ionization probability of $29\,^3S$ atoms as a function of on-axis field amplitude in cavity *I*. The curve is composed from three separate measurements on overlapping field amplitude intervals.

tion curve of atoms prepared in the $(n_0=29)^3S$ state. In order to bring out the threshold region more clearly, the ionization rate was measured in three overlapping intervals which are shown overlayed. Overlaying is necessitated by the finite dynamic range of our linear power sweep circuitry and by the quadratic relation between the linearly scanned power and the field strength Eq. (2). Between the onset of ionization at a field amplitude of 75 V/cm, and saturation of the ionization signal at 1200 V/cm, rich structure can be observed. The threshold region is shown enlarged in Fig. 4. Similar oscillatory structure can be observed in the threshold ionization behavior of $(n_0=26)^3S$ states in Fig. 5. Unfortunately, because the saturation of the ionization rate would take place at field strengths beyond the range of available microwave power (20 W), the vertical scale in Fig. 5 could not be normalized.

The label voltage applied to the cavity in the ionization mode experiments induces stray (mostly longitudinally directed) electric fields near the entrance and exit holes in the cavity endcaps. These static fields, however, drop quickly on a length scale of a hole diameter inside the cavity. Small changes in the detailed shape of the measured ionization curves were observed when the label voltage was varied. Similar effects occasionally resulted from variation of other experimental parameters, such as beam steering.[19]

B. Excitation experiments

For the excitation measurements atoms were prepared in $n_0\,^3S$ states, interacted with the microwave field, and subsequently traversed the longitudinal ionizer. The ion current produced by this static electric-field ionizer was measured as a function of the on-axis field amplitude in the cavity. The voltages on the ionizer electrodes were set just beyond the threshold for static field ionization of $(n_0, M_L=0)$ states. A key point in the interpretation of these experiments is that atoms that survived the interaction with the ionizer field, that is, the complement of the measured signal, were atoms promoted to states of high angular momentum inside the cavity.

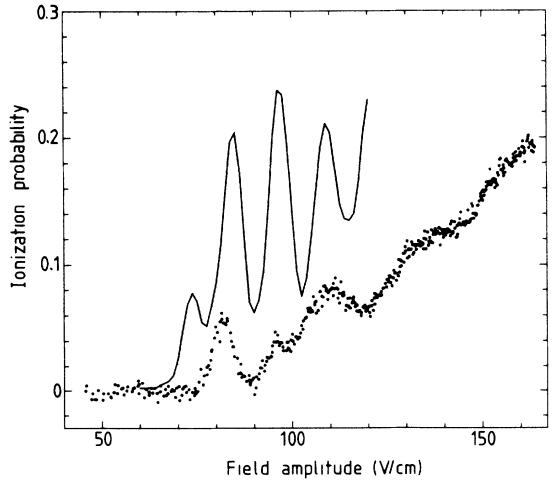

FIG. 4. Microwave ionization probability of $29\,^3S$ atoms as a function of field amplitude. Dots: enlargement of the threshold region of Fig. 3. Solid line: $29\,^3S \rightarrow \sum_{l=0}^{29} 30\,^3l$ transition probability after three cycles of the field computed from a numerical integration of the time-dependent Schrödinger equation.

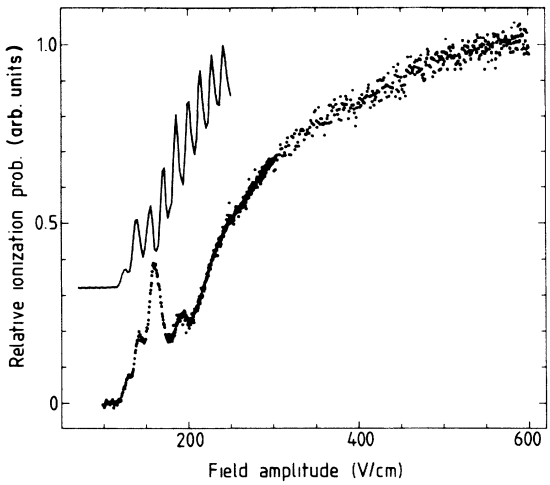

FIG. 5. Microwave ionization probability of $26\,^3S$ atoms as a function of field amplitude in cavity I. Dots: unnormalized experimental result. Solid line: $26\,^3S \rightarrow \sum_{l=0}^{26} 27\,^3l$ transition probability after three cycles of the field computed from a numerical integration of the time-dependent Schrödinger equation. The calculated transition probability has a maximum of 0.35.

1. *Selective detection of high-angular-momentum Rydberg atoms*

The evidence substantiating this assumption may be appreciated by briefly recalling the static electric-field ionization mechanism for nonhydrogenic states.[15,21] An electron in a hydrogen atom that is placed in a region of static electric field is described by parabolic wave functions (channels). In each of those channels the atom decays through tunneling of the electron towards the anode. The decay rate increases quickly with the field strength and depends upon the parabolic quantum numbers: Channels whose energy decreases most with increasing field strength ionize most rapidly. For those channels the threshold field scales with n as $F_{\rm thr} \simeq 0.1 n^{-4}$, whereas for channels whose energy increases most with increasing field, the most stable channels, $F_{\rm thr} \simeq 0.3 n^{-4}$.[20] In nonhydrogenic atoms the parabolic channels are coupled by the interaction between the excited electron and the core electrons; their coupling strength V is expressed directly in the quantum defects μ_l [in cases with a single nonzero μ_l, $V \simeq \tan(\pi\mu_l)$].[21] This core-induced coupling of channels is responsible for a marked difference between the ionization behavior of $M_L=0$ states and states with $|M_L| \gtrsim 2$, states whose wave functions have a much smaller overlap with the atomic core. Atoms prepared in states with small values of the azimuthal quantum number will have an ionization threshold given by $F_{\rm thr} \cong \frac{1}{16} n^{-4}$, which is precisely the locus (in field strength and energy) of strong overlap between narrow (almost stable) and broad (rapidly decaying) parabolic channels.

Conversely, states with $|M_L| \gtrsim 2$ will behave hydrogenically, except perhaps at isolated values of the field strength where narrow and broad channels mix.

2. *Quench mode measurements*

Figure 6(a) shows the survival probability of $(n_0=30)^3S$ atoms that have been exposed to the microwave electric field, as a function of field amplitude. The field strength inside the (downstream) longitudinal ionizer was set just beyond the ionization threshold for $30\,^3S$ atoms. At a power of about 34 μW the signal shows a sharp dip and transitions apparently occur out of the initial state to final states that ionize at higher ionizer field strengths. Because the value of the field strength inside the ionizer is only approximately known, these final states were analyzed by static field ionization in a region

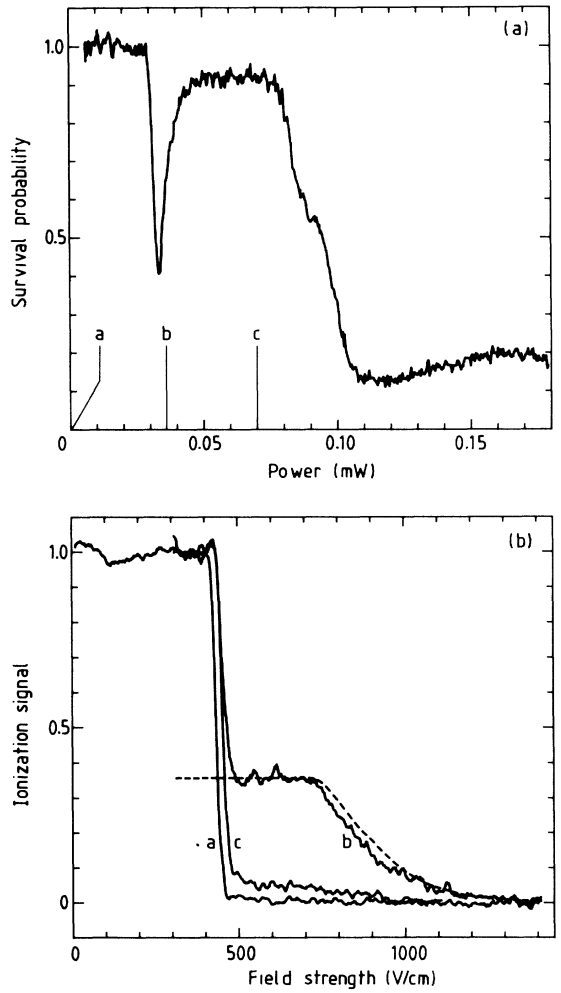

FIG. 6. (a) Survival probability of He $30\,^3S$ atoms as a function of microwave power dissipated in cavity *II*. (b) Analysis of the substate distribution by static field ionization of atoms that have been subjected to microwave fields with power settings of 0, 36, and 70 μW, indicated as *a*, *b*, and *c*, respectively. Dashed line: Monte Carlo simulation of the ionization behavior of $n=30$ hydrogen atoms equally distributed over all possible L and M_L substates.

of precisely known electric-field strength F_a between the cavity and the longitudinal ionizer. To this aim the field strength inside the ionizer was set high enough so that all atoms with $n \geq 30$, including those with $M_L \neq 0$, were ionized and detected. Roughly, the strength of this signal will decrease as F_a approaches the maximum field strength inside the ionizer and more and more excited atoms will be removed from the beam.

Figure 6(b) shows the signal as a function of analyzer static field strength F_a at three settings of the microwave power. The three curves are normalized to unity at $F_a=0$ where all atoms emerging from the cavity were detected, and to zero at $F_a=1400$ V/cm, where no atom survived to be detected. At a microwave power of 36 μW, the analyzer signal exhibits a plateau followed by a tail; the height of the plateau equals the complement of the microwave quench signal at 36 μW. The shape of this curve was compared to the result of calculations of the ionization threshold of hydrogen atoms based on the semiempirical formula given by Damburg and Kolosov.[20] We carried out a Monte Carlo calculation that simulated an ensemble of hydrogen atoms uniformly distributed over all possible substates of the $n=30$ manifold. As may be judged from Fig. 6, such a distribution is consistent with the observed ionization curve. The graphs of the ionization probability at zero microwave power and that at 70 μW have the same sharp decrease in signal at about 425 V/cm, which is characteristic for static field ionization of $30\,^3(M_L=0)$ "nonhydrogenic" states.

This experimental observation is consistent with our hypothesis that atoms were excited *inside* the cavity from $(n_0=30)^3S$ states to $30\,^3L, L \gtrsim 2$ $(M_L=0)$ states, which then evolved *after* the cavity into states of large $|M_L|$. The idea is that once the excited atoms emerged from the cavity exit aperture, and traversed a region of (small) stray electric fields these high-L states did not preserve their $M_L=0$ quantum number with respect to the transverse quantization axis provided by the electric field F_a inside the substate analyzer. Instead, either interaction with the stray fields, or the spin-orbit interaction, or both, induced transitions to states with all possible M_L values. To produce hydrogenic Stark ionization behavior in helium Rydberg atoms at our experimental conditions one needs only $|M_L| \gtrsim 2$. The same principle governs the detection of excited atoms by ionization inside the longitudinal ionizer which is located even further downstream from the cavity.

The results shown in Fig. 6(b) also suggest the procedure that was followed for normalizing quench-mode experiments, which includes that of Fig. 6(a). These spectra were normalized to unit survival probability at zero microwave power, and to zero survival probability in a section in each scan (that is not shown) where F_a was switched from zero to a field strength that, in the case of $n_0=30$, exceeded 1400 V/cm.

3. *Unquench mode measurements*

From the above it may be evident that a decrease in signal in the quench mode is not only caused by microwave-induced transitions to states which are harder

to ionize (states with high $|M_L|$ that have evolved from states with high L), but also by promotion to states which will already ionize inside the cavity. This could be convincingly demonstrated in yet another mode of operation, which we introduced as the "unquench" mode.

In this mode the static analyzer field strength F_a is set slightly beyond the threshold value for ionizing $n_0\,^3S$ atoms, whereas the ionizer field was set at saturation strength. Consequently, the ion signal will only be nonzero when atoms are promoted to states whose static ionization threshold field exceeds F_a, in particular, atoms that were promoted to high L ($|M_L|$) states. The unquench signal, therefore is the complement of the quench signal, except when the microwave electric-field amplitude is set beyond the microwave ionization threshold of $n_0\,^3S$ atoms. This effect is shown in Fig. 7 where the survival probability of $(n_0=26)^3S$ atoms is shown together with the complement of the unquench signal, which was measured with F_a set to 942 V/cm. The two curves start to deviate at a microwave field amplitude $F_0=140$ V/cm. Comparison with Fig. 5 shows that this field amplitude precisely signifies the onset of microwave ionization of $(n_0=26)^3S$ atoms.

4. Results

Figures 8(a) and 8(b) show the survival probability as a function of the microwave electric-field amplitude on the cavity (beam) axis for each n_0 value in the range 25–32. In each case the field strength inside the longitudinal field ionizer was set such that it detected $n_0\,^3S$ atoms, but did not detect $(n_0, |M_L| \gtrsim 2)$ atoms, as described above. The analyzer field F_a was set to zero except briefly during each scan for normalizing the spectrum. All curves were measured using cavity *IV*, where the field is turned on in about 30 microwave cycles. Almost all curves are marred by sharp structures, in a few cases the depth of which corresponds to a microwave induced transition probability of 0.8. The noise in the spectra varies with the efficiency of the excitation scheme that was used to prepare atoms in initial $n_0\,^3S$ states. Each noisy spectrum had to be averaged over many repeated scans of the microwave power during a few hours of data collection. In all cases the observed structures tend to broaden at the higher field strengths. We will shown in Sec. IV B that this phenomenon is connected to the switching transient $A(t)$ of the microwave electric-field amplitude in the

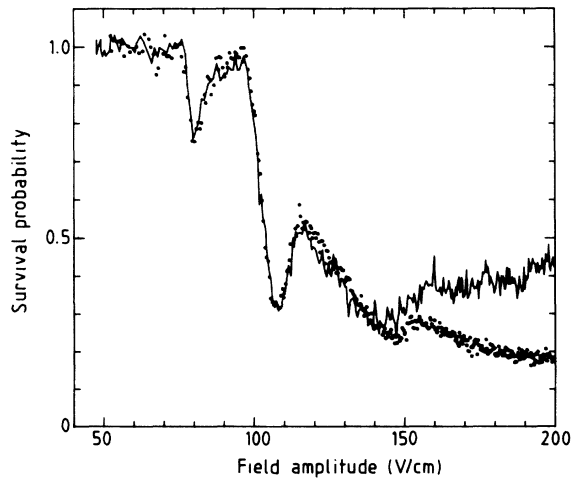

FIG. 7. Dots: survival probability ("quench" signal) of He $26\,^3S$ atoms as a function of on-axis microwave field amplitude inside cavity *II*. Solid line: complement of an "unquench" signal (see text).

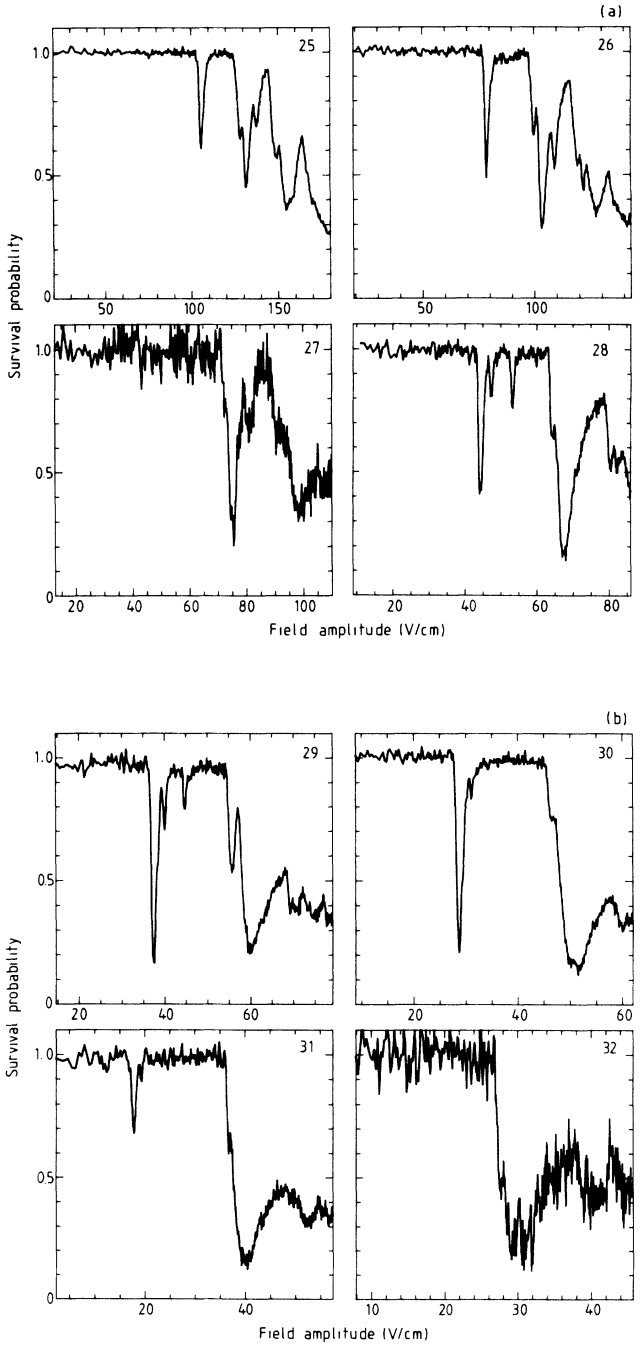

FIG. 8. (a) Survival probability of helium $n_0\,^3S$ atoms, $n_0=25$–28, as a function of the on-axis electric field amplitude inside microwave cavity *IV*. (b) Survival probability of helium $n_0\,^3S$ atoms, $n_0=29$–32, as a function of the on-axis electric field amplitude inside microwave cavity *IV*.

moving atomic rest frame. We also emphasize that the sharp structures were observed *well below* the field strength where ionization sets in, and where, necessarily, mixing with adjacent n_0-1 and n_0+1 manifolds would take place. For example, Fig. 4 (5) shows that microwave ionization of $n_0=29$ $(n_0=26)^3S$ atoms began at a microwave amplitude F_0 of about 75 V/cm (120 V/cm), whereas Fig. 8(b) [8(a)] shows that the first occurrence of strengths for $n_0=29$ $(n_0=26)^3S$ atoms is at about 37 V/cm (77 V/cm). In Sec. IV we analyze the spectra for $n_0=28$ and 29 in more detail.

IV. INTERPRETATION

A. Ionization experiments

Figure 9 shows a calculated spectrum of energies fanning out of the triplet helium $n=26$, $M_L=0$, manifold as a function of static electric-field strength. At a field strength of about 130 V/cm, levels of the $n=26$ manifold exhibit their first anticrossings with levels descending from the next higher $n=27$ manifold, whereas ascending levels of the next lower manifold are first encountered at about 160 V/cm. The observed onset of microwave ionization of $(n_0=26)^3S$ atoms (see Fig. 5) is located close to the smallest of these two values of the field amplitude, whereas the observed structure extends beyond the largest of the two values.

This correlation suggests that ionization is mediated by excitation from the initial n_0 to the next higher n_0+1 manifold. In a quasistatic view, in which the levels drawn in Fig. 9 adapt almost adiabatically to the instantaneous electric field, such transitions would take place in two phases during a field cycle. First, population would be transferred from the downward bending $(n_0=26)^3S$ state to upward going states [i.e., states whose energy increases as $|F(t)|$ increases] of the same manifold when the field reverses sign and is changing fastest. Next, the downward going states of the next higher manifold would be reached when the instantaneous electric field traverses the region of anticrossings between the $n_0=26$ and $n=27$ manifolds.

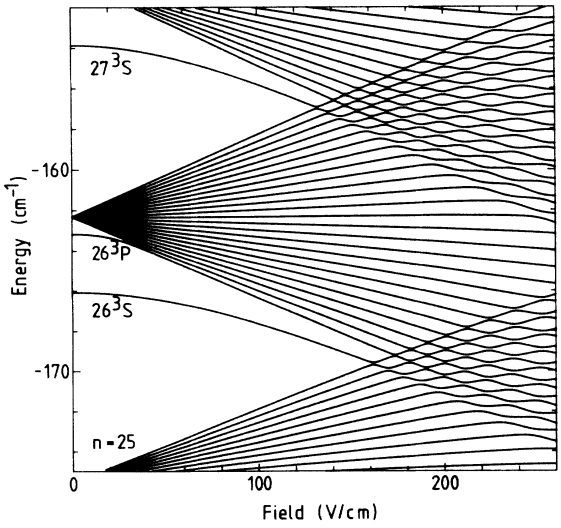

FIG. 9. Plot of helium triplet $M_L=0$ energy levels in a static electric field as a function of field strength.

Analogous to the description of an atomic collision process in terms of (quasistatic) molecular potential curves, it may be tempting to assign a key role to individual anticrossings between Stark states and to evaluate transition probabilities at those anticrossings using the Landau-Zener-Stückelberg (LZS) formula.[22] However, because the rate of change of the field (analogously, the relative velocity of the partners in an atomic collision) is high, an argument first put forward by Bates[23] shows that in our case transitions are not at all restricted to isolated anticrossings in Fig. 9.

Directly adapting this argument, the influence of an anticrossing is felt over a field interval ΔF that is given by

$$\Delta F=\left[\frac{4\pi s dF/dt}{d(\Delta E)/dF}\right]^{1/2}, \tag{3}$$

where ΔE is the energy difference between the diabatic crossing states, dF/dt the rate of change of the field, and $s>1$ is a number defined below. Equation (3) expresses that when the field sweeps through the transition region, the phase difference between the wave functions of the crossing states should increase by a few (s) time π. Substitution in Eq. (3) of typical values $d(\Delta E)/dF=10^{-1}$ cm^{-1}/(V/cm); $dF/dt=\omega F_0\cos\omega t$, $F_0=130$ V/cm, and $s=2$ gives maximal values of $\Delta F\cong 100$ V/cm when $\omega t=0,\pi$. This is much larger than the extent of isolated anticrossings such as shown in Fig. 9. Only when the amplitude of the oscillating field is set *just beyond* an anticrossing will it be traversed slowly enough that one may hope to see an effect due to this particular anticrossing alone. For example, Eq. (3) implies that the transition region $\Delta F\cong 10$ V/cm, approximately the spacing of anticrossings in Fig. 9, only when ωt is very close to $\pi/2$, or, conversely, when the instantaneous field strength is within 1 V/cm of its maximum value. We conclude that application of the LZS formula to calculate transition probabilities is prohibited.[24]

An estimate of the transition probability for transitions between an n ^3S state and states of the $n+1$ triplet manifold thus should involve *many* interacting Stark states of both manifolds. A peculiarity of the system studied here is that the quantum defect of the ^3S state is rather large $(\mu_0=0.269)$.[25] This means that *direct* transfer of population from the n_0 ^3S states to rising states of the same manifold, which would occur when the field $F(t)$ reverses sign, is unlikely. Such population transfer may, however, be enhanced when both n_0 ^3S and n_0 $^3L>0$ states mingle with states of the next lower manifold when the field reaches out to the region of anticrossings between the n_0 and n_0-1 manifold. Consequently, and perhaps paradoxically, an estimate of the probability for transitions upward from n_0 should also include Stark states of the *lower* n_0-1 manifold.

The integration of the time-dependent Schrödinger equation on a basis of many states can in this case be set

up most efficiently by selecting diabatic (parabolic) basis states. The core-induced interaction between the members of this basis can be expressed directly in terms of the quantum defects through a geometrical factor.

The Schrödinger equation for a nonhydrogen Rydberg atom in a sinusoidally varying electric field is approximately

$$i\frac{d\Psi}{dt}=[H_0+V+zF(t)]\Psi\equiv H(t)\Psi\ ,$$
$$F(t)=F_0\sin(\omega t)\ , \tag{4}$$

where H_0 is the zero-field nonrelativistic hydrogen Hamiltonian, F_0 and ω are the amplitude and frequency of the electric field, and a spherically symmetric V approximates the interaction of the excited electron with the He core. We next expand the time-dependent He wave function in eigenfunctions of H_0+zF for constant field that parametrically depend on field (time)

$$\Psi(t)=\sum_i c_i(t)\phi_i(F(t))\ , \tag{5}$$

which upon substitution in Eq. (4) gives

$$i\frac{dc_i(t)}{dt}+i\sum_j\left\langle\phi_i\left|\frac{d}{dF}\right|\phi_j\right\rangle\frac{dF}{dt}c_j(t)-\sum_j V_{ij}c_j(t)$$
$$=E_i(F(t))c_i(t)\ . \tag{6}$$

For the relatively small field strengths of interest here, the $|\phi_i\rangle$ may be approximated by zero-field parabolic wave functions, whose Stark-shifted energies vary linearly with the field. In that case Eq. (6) reduces to

$$i\frac{dc_i(t)}{dt}-\sum_j V_{ij}c_j(t)=E_i(t)c_i(t)\ ,$$

with

$$E_i(t)=\varepsilon_i+\eta_i F_0\sin(\omega t)\ ,$$
$$\eta_i=\tfrac{3}{2}n_i(n_{1_i}-n_{2_i})\ , \tag{7}$$

where $\varepsilon_i=-1/2n_i^2$ is the zero-field hydrogenic energy, n_1 and n_2 are parabolic quantum numbers, and $V_{ij}=\langle\phi_i|V|\phi_j\rangle$. After removal of a common phase factor we obtain

$$i\frac{db_i(t)}{dt}-\sum_j\exp\left[-i\int^t[E_j(\tau)-E_i(\tau)]d\tau\right]V_{ij}b_j(t)=0\ , \tag{8}$$

where

$$b_i(t)=c_i(t)\exp\left[i\int^t E_i(\tau)d\tau\right]\ .$$

For two crossing states $|\phi_1\rangle,|\phi_2\rangle$ and a linear function $F(t)$, Eq. (8) yields an analytic solution in terms of Weber functions. The Landau-Zener-Stückelberg formula then expresses the transition probability between coupled states which, far from their anticrossing, have asymptotically joined the $|\phi_1\rangle,|\phi_2\rangle$.[22]

The phase integral in Eq. (8) can be performed analytically and the set of coupled first-order differential equations for the complex amplitudes $b_i(t)$ can be integrated readily using a standard numerical package.[26] A strictly identical theory can be based upon eigenfunctions of H_0+V+zF instead. However, a calculation on this adiabatic basis would retain the second term in the left-hand side of Eq. (6), and appears to be numerically more problematic.

The matrix elements of the spherically symmetric core interaction V_{ij} were first evaluated on a zero-field hydrogenic basis $|n,l,m\rangle$ and next transformed to a parabolic basis $|n,n_1,n_2\rangle$ using a standard geometrical transformation[27]

$$|n,n_1,n_2\rangle=\sum_{l=|m|}^{n-1}\left\langle\frac{n-1}{2},\frac{n-1}{2},\frac{m+n_1-n_2}{2},\frac{m+n_2-n_1}{2}\middle|l,m\right\rangle|n,l,m\rangle \tag{9}$$

in terms of Clebsch-Gordon coefficients. A first estimate of the diagonal matrix elements of the core interaction would be

$$\langle n,l|V|n,l\rangle=E_{nl}-\varepsilon_n=-\frac{1}{2(n-\mu_l)^2}+\frac{1}{2n^2}\cong-\frac{\mu_l}{n^3}\ , \tag{10}$$

where E_{nl} are the zero-field He energies and μ_l are the He quantum defects. Komarov, Grozdanov, and Janev generalized this simple result to off-diagonal matrix elements[28]

$$\langle n,l|V|n',l\rangle\cong-\frac{\mu_l}{(nn')^{3/2}}\ . \tag{11}$$

It turns out that Eq. (11) [together with Eq. (9)] predicts approximately the correct level separation at anticrossings between states of adjacent n and n' manifolds. It is obvious, however, that Eqs. (10) and (11) give an error in the zero-field energies of two or more interacting manifolds because their proper value would already be given by the diagonal elements of V alone [Eq. (10)]. Because in our case transitions at zero instantaneous field as well as those in the region of anticrossings, where the instantaneous field is near its extremal values, are important, we have sought to cure this shortcoming. Our approach is essentially an approximation of the optical potential which results from restricting the parabolic basis set to a few, say N, manifolds. It is outlined in Appendix A. An exact expression for the matrix elements between parabolic channels has been given by Harmin.[21] Those matrix elements, however, do depend upon the energy of the channels.

The solid curves in Figs. 4 and 5 show, respectively, the transition probabilities $P[n\,^3S\rightarrow\sum_{l=0}^{n}(n+1)^3l]$ for

$n=29$ and 26. They were evaluated by an incoherent sum over substates. Each calculation started the system of equations Eq. (8) with unit population in the $n_0\,{}^3S$ state at $t=0$. This initial condition was transformed to the parabolic basis using the matrix which diagonalizes H_0+V [Eq. (4)], whereas its adjoint was used when examining the redistribution of population after three cycles of the field. All states of the n_0-1, n_0, and n_0+1 manifolds were included, giving rise to 174 coupled real differential equations in the case of $n_0=29$.

Although a time interval of three field cycles is quite arbitrary (and short), each model calculation does approximately reproduce the threshold field amplitude and an oscillatory behavior of the transition probability past the threshold. The spacing of the computed maxima of the transition probability approximately reproduces the spacing of the structures observed experimentally in Figs. 4 and 5. An important difference is that the measured structures, especially those in Fig. 5, die out after a few oscillations of unequal amplitude, whereas the calculated oscillations persist. We presume this difference is due to the finite integration time and the limited basis used in the present model. A comparison between Figs. 5 and 9 shows that in case of $n_0=26$ the period of the oscillatory excitation probability is approximately twice the field interval between two consecutive anticrossings. At first sight a surprising conclusion then is that some of the individual character of the anticrossings remains in this (necessarily) multistate approach. However, it should be kept in mind that this character will only be felt when the anticrossings are located very close to the crest of the field. We conjecture that the oscillatory structure above threshold in the ionization curves is caused by interferences between many coherently excited almost adiabatic Stark states whose coupling is more or less localized near anticrossings. The array of regularly spaced anticrossings may then act as a wave-mechanical diffraction grating.

Finally, we notice that the calculations predict a nonnegligible $n\,{}^3S\rightarrow n+1$ transition probability $[O(0.1)]$ after only three field cycles. The relevance of this number remains, however, unclear because many such $n\rightarrow n+1$ transitions must be made along the way to the ionization continuum and probably also a fair amount of population may be trapped (at least temporarily) in lower manifolds by deexcitation. For example, in our $n_0=26$ model calculation, the $n_0\,{}^3S\rightarrow n_0-1$ deexcitation probability after three cycles exceeds the probability for excitation at field amplitudes larger than 140 V/cm, it rises as large as 0.8 at 170 V/cm and shows similar oscillatory structure.

The steplike appearance of microwave ionization curves such as those shown in Fig. 3 may be connected with the population dynamics sketched in the preceding paragraph. Another candidate explanation for this remarkable phenomenon is the possible population of states with $|M_L|>0$ through the effect of spin-orbit coupling. Although the spin-orbit precession time is large with respect to the field period, the importance of spin-orbit effects can only be assessed through a more careful analysis and appropriate experiments. (The precession time at $n=30$ is 3×10^{-8} s, decreasing as n^{-3} with increasing n.[25])

B. Excitation experiments

In principle, the analysis of the intra-n_0-manifold excitation experiments could be conducted along the same lines. Integration of the time-dependent Schrödinger equation on a basis of the $n_0=28$ manifold alone results in Fig. 10, which shows the transition probability $P(28\,{}^3S\rightarrow\sum_{l=3}^{27}28\,{}^3l)$ as a function of the field amplitude. The transition probability was computed by starting the integration of Eq. (8) at $t_0=0$ with unit popula-

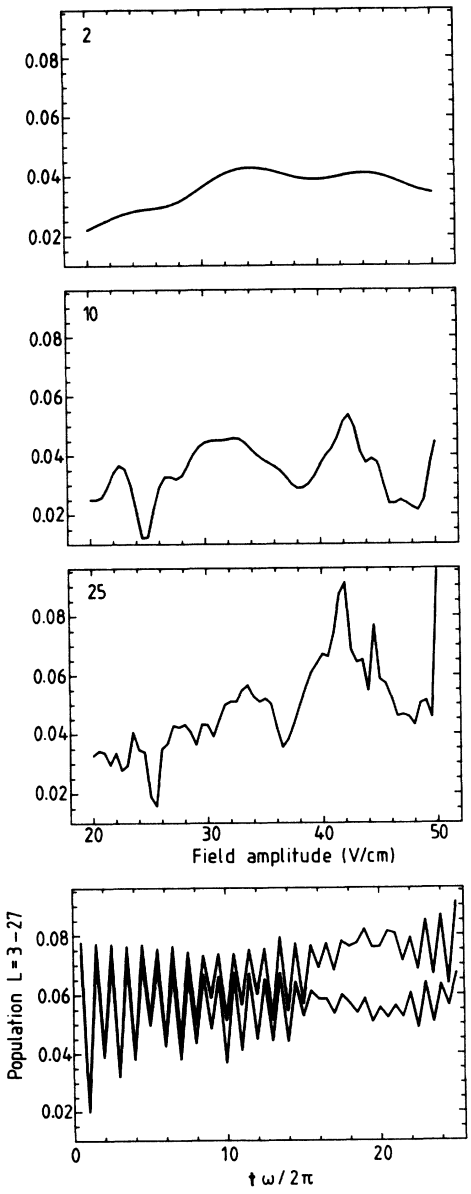

FIG. 10. Calculated transition probability $28\,{}^3S\rightarrow\sum_{l=3}^{27}28\,{}^3l$ by integrating the time-dependent Schrödinger equation for $n=28$ atoms in a sinusoidal field. Top three graphs: as a function field amplitude after 2, 10, and 25 cycles of the field, respectively. Bottom graph, lower curve: as a function of time at 40 V/cm field amplitude; upper: at 42 V/cm.

tion in the $28\,^3S$ state, and examining the incoherently summed population $\sum_{l=3}^{27} 28\,^3l$ after a number of cycles ($t=4\pi/\omega$, $20\pi/\omega$, and $50\pi/\omega$, respectively). During the integration of 56 coupled equations of the $n=28$ manifold, the total population remained conserved to within 10^{-5}. Although the choice of those integration times is arbitrary, the development of a resonance at about 42 V/cm is clearly visible. The lowest frame in the figure shows that after about 20 cycles the summed population $\sum_{l=3}^{27} 28\,^3l$ at resonance (42 V/cm) starts to diverge from its value off resonance (40 V/cm). Quite contrary to what was observed for the short-time *inter-n*, $n \rightarrow n+1$ population transfer, the *intra-n* transition probability after a few cycles is a smooth function of field amplitude. This again illustrates that the threshold structure of ionization curves is more strongly tied to the structure of atoms in a *static* electric field. On the other hand, the structure in the intramanifold transition probability is a true, long-time resonance effect.

It is quite straightforward to allow for the field-envelope function $A(t)$ in this explicit time-dependent method and to extend the integration time to the full interaction period. However, such procedure fails to capture the essential physics in the problem—namely, that there are two disparate time scales, one associated with the fast $\sin(\omega t)$ since dependence of the instantaneous electric field, and a much slower one with the rise and fall of the field envelope function $A(t)$. The existence of these time scales may be appreciated by realizing that for the field amplitude to rise from 10% to 90% of its maximum value it takes 80 and 30 oscillations of the instantaneous electric field in cavity *II* (*III*) and *IV*, respectively.

1. *Floquet analysis*

The separation of the time scales of the transient microwave field can be achieved by removing the fast $\sin(\omega t)$ time dependence through a Floquet analysis.[29] Floquet's theorem states that for a periodic $F(t)$, the solution to Eq. (4) can be written as

$$\Psi(t)=\Phi(t)e^{-iQt} , \tag{12}$$

where Q is a diagonal matrix, and Φ is a matrix of periodic functions that may be expanded in a Fourier series

$$\Phi_{\alpha\beta}(t)=\sum_k \Psi^k_{\alpha\beta} e^{ik\hbar\omega t} . \tag{13}$$

The so-called quasienergy states $\Psi^k_{\alpha\beta}$ are eigenvectors of the time-independent Floquet Hamiltonian H^F with eigenvalue, say, $q_{\beta,0}$

$$\sum_{\gamma,m} \langle \alpha,k|H^F|\gamma,m\rangle \Psi^m_{\gamma\beta}=q_{\beta,0}\Psi^k_{\alpha\beta} ,$$

with

$$\langle \alpha,k|H^F|\gamma,m\rangle = H^{k-m}_{\alpha\gamma}+k\hbar\omega\delta^\gamma_\alpha\delta^m_k , \tag{14}$$

where $H_{\alpha\beta}$ are the Fourier coefficients of the electric field $H_{\alpha\beta}(t)=\sum_k H^k_{\alpha\beta}e^{ik\hbar\omega t}$, with k a Fourier index. The significance of the Floquet Hamiltonian may be appreciated by interpreting the states $|\alpha,k\rangle$ as direct products of atom $|\alpha\rangle$ and photon number $|k\rangle$ states. This interpretation is consistent with the semiclassical approximation of the radiation field, applicable when the photon number is large so that its fluctuations due to absorption and emission are negligible.[29]

The periodicity of the field endows the spectrum of the Floquet Hamiltonian with periodic properties. With $q_{\beta,0}$, all $q_{\beta,k}$ are also quasienergies

$$\begin{aligned} &q_{\beta,k+p}=q_{\beta,k}+p\hbar\omega , \\ &\langle \alpha,k|q_{\beta,m}\rangle=\langle \alpha,k+p|q_{\beta,m+p}\rangle . \end{aligned} \tag{15}$$

where $|q_{\beta,m}\rangle$ indicates the eigenvector that accompanies the eigenvalue $q_{\beta,m}$. In practice, the Floquet matrix must be truncated and the periodic properties Eq. (15) will only approximately hold in the central part of its spectrum.

Maquet, Chu, and Reinhardt have pointed out that the Floquet matrix can be organized efficiently by including only those atom-photon states that possess the same parity as the initial state [the parity equals $(-1)^{L+k}$, where L is the atomic angular momentum and k is the photon number].[30] For clarity we show the structure of the even-parity Floquet matrix in the case of four angular momentum states ($L=0$–3),

$$\begin{pmatrix} S & V_{ps} & & & & V_{ps} \\ V_{sp} & P-\omega & V_{dp} & & & \\ & V_{pd} & D & V_{fd} & & V_{pd} \\ & & V_{df} & F-\omega & & \\ & & & & S+2\omega & V_{ps} \\ V_{sp} & & V_{dp} & & V_{sp} & P+\omega \cdots \end{pmatrix} , \tag{16}$$

where the symbols $P-\omega$ denote the energy of the $L=1$ angular momentum states minus the photon energy $\hbar\omega$, and where V is the product of the field amplitude and half the dipole matrix element $V_{l,l+1}=F_0\langle \alpha_l|r|\alpha_{l+1}\rangle/2$. These matrix elements were computed from the quantum defects of triplet helium states using a method that originates from Bates and Damgaard.[31] Figure 11 shows a little more than one period of the spectrum computed for $n=28$, using a basis set consisting of 28 atomic states ($n=28$, $l=0$–27, $M_L=0$) with 25 photon states. Because the basis only includes states with even parity, the periodicity of the spectrum is $2\hbar\omega$ (0.6620 cm^{-1}). The spectrum is characterized by ubiquitous anticrossings as is clearly seen in an enlarged section of the spectrum shown in Fig. 12.

The price of losing the explicit time dependence of the problem is that the total number of photon states of the Floquet matrix is unknown. This number should be chosen large enough such as to ensure convergence of the middle part of the spectrum at the highest field amplitude.[32] The following simple argument shows that for an isolated manifold the needed number of photon states increases linearly with the field amplitude.[33] They key point is that in the linear Stark regime the Floquet spectrum of the hydrogen atom is exactly

$$\langle \alpha k|q\rangle = J_k(F_0\eta_\alpha/\omega) , \tag{17}$$

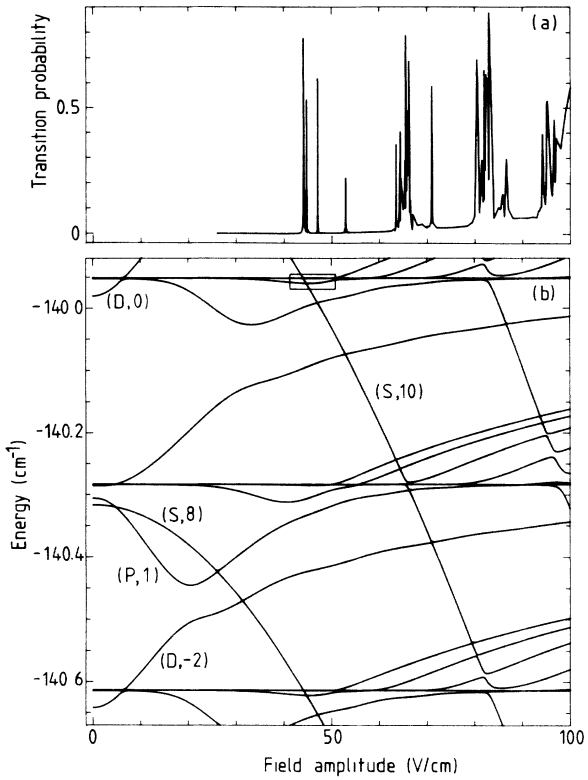

FIG. 11. (a) Computed transition probability $28\,^3S \rightarrow \sum_{l=3}^{27} 28\,^3l$ using Eq. (20) and the adiabatic initial state indicated in (b) as $(S,8)$ and $(S,10)$. (b) Map of quasienergy levels of He $28\,^3S$ atoms subjected to a 9.924-GHz microwave electric field as a function of field amplitude. The spectrum is periodic in $2\hbar\omega$. The part of the spectrum inside the small box is shown enlarged in Fig. 12.

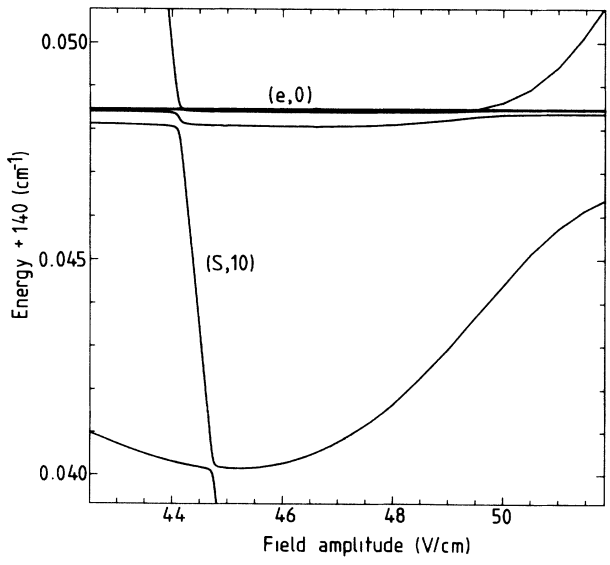

FIG. 12. Enlargement of a part of the quasienergy spectrum in Fig. 11 (there indicated by a small box), showing the anticrossings that are responsible for the first peaks in Fig. 11(a).

where η_α is the linear polarizability of the (parabolic) atomic state α [see Eq. (7)]. For large photon numbers k, we may substitute the following asymptotic expansion for the Bessel function J_k:[34]

$$J_k(F_0\eta_\alpha/\hbar\omega) \cong \frac{1}{(2\pi k)^{1/2}} \left[\frac{eF_0\eta_\alpha}{2k\hbar\omega} \right]^k , \tag{18}$$

where e is the base of the natural logarithm. We expect that convergence with k of the Floquet calculation is a result of the decrease of J_k to a sufficiently small value for large enough photon numbers. For large k, the locus of constant magnitude of the Floquet matrix elements is obviously dictated by the second factor in Eq. (18),

$$F_0\eta_\alpha \simeq k\hbar\omega , \tag{19}$$

which shows that the extent of the hydrogen-Floquet spectrum is proportional to the linear Stark shift in a *static* electric field. We expect that these considerations in an approximate sense also apply to the nonhydrogenic case.

Here it may be enlightening to discuss the relation between anticrossings of static Stark levels and those occurring in quasienergy spectra. Equation (19) suggests that the field strength where anticrossings first occur between extremal states of different manifolds is proportional to the field amplitude where quasienergy states of different manifolds n and $n+1$ overlap. In other words, the field amplitude where the Floquet matrix ceases to be factorizable, in a part only involving n and a part only involving $n+1$, scales with the static field where anticrossings between the n and $n+1$ manifolds first occur. It is obvious that this argument only applies to the gross structure of the Floquet matrix (on a scale $\hbar\omega$). At smaller scales, the effects of the core interaction dominate the structure of the quasienergy spectrum of nonhydrogenic atoms. Therefore this argument may only be used to approximately locate the field amplitude where $n \rightarrow n+1$ transitions may occur for the first time. The proper value of this amplitude, however, is dictated by anticrossings of quasienergy states. This is immediately evident from the phenomenology of the intra-n excitation processes discussed in this paper, where there are strong multiphoton resonances at field amplitudes which are not anywhere near avoided crossings between levels in a static field.

We are, therefore, quite skeptical about the value of a conclusion, reached by van Linden van den Heuvell *et al.*, that the Landau-Zener-Stückelberg formula and the photon (Floquet) picture should be two equivalent ways of viewing the present problem.[11,12,33] The statement is, maybe trivially, correct in the sense that, in case of a harmonic field variation, the time-dependent approach [Eq. (8)] is strictly identical to the time independent theory [Eq. (14)]. In fact, this notion is implicit in a version of Floquet theory that is based upon the propagator over one field period (the so-called monodromy operator).[35] However, as has been argued in Sec. IV A, the statement is not correct in the following sense: excitation processes of Rydberg atoms in a microwave electric field definitely do *not* remain confined to isolated values of the static field strength where two states avoid crossing.

Using the periodic property of the Floquet matrix, the time-dependent transition probability of exciting an initial state $|\alpha,0\rangle$ to final $|\beta,k\rangle$ atom-photon states can be written as

$$P_{\beta\leftarrow\alpha}(\tau)=\sum_{k}\sum_{\substack{\gamma,m\\ \gamma',m'}}\langle\beta,k|q_{\gamma,m}\rangle\langle q_{\gamma,m}|\alpha,0\rangle\langle\alpha,0|q_{\gamma',m'}\rangle \times\langle q_{\gamma',m'}|\beta,k\rangle e^{i(q_{\gamma m}-q_{\gamma' m'})\tau}, \quad (20)$$

which has been summed over the final-state photon number k. The relevance of Eq. (20) is that the transition probability is only non-negligible if both the initial $|\alpha,0\rangle$ and the final $|\beta,k\rangle$ states have a significant overlap with eigenstates $|q_{\gamma,m}\rangle$ and $|q_{\gamma',m'}\rangle$ of the Floquet matrix. In other words, transitions occur at anticrossings of two eigenenergies of the Floquet matrix.[36] Therefore only a few terms in the sum of Eq. (20) actually contribute. It should also be noted that the periodicity of the Floquet Hamiltonian gives the "photon numbers" in Eq. (20) only a relative status: it is irrelevant where in the spectrum $k=0$ is chosen. This is, of course, in accord with the interpretation of the Floquet Hamiltonian as a model for a semiclassical radiation field.

A crucial aspect of the problem that is not made explicit in Eq. (20) is how the bare atomic state $|\alpha\rangle$ is turned into atom-field states $|\alpha,k\rangle$ when the field is switched on, and how the states $|\beta,k\rangle$ are turned into a bare state $|\beta\rangle$ when the field is switched off. In fact, Eq. (20) implies that the turn-on and turn-off are sudden with respect to $|\alpha\rangle$ and $|\beta\rangle$, and adiabatic with respect to all other atomic states. If only two states were to contribute, Eq. (20) would become the well-known Rabi formula.[37] We will now explain how this notion of the underlying dynamics may be refined.

The key quantity determining the adiabaticity of the field turn-on is the ratio of the rate of change of the quasienergies, caused by the field amplitude changing via $A(t)$, to the inverse width of anticrossings between quasienergy states (which equals the Rabi frequency for pairwise anticrossings). When the changing amplitude causes the quasienergies to change rapidly with respect to an inverse anticrossing width, that anticrossing will be traversed diabatically. A first crude distinction between adiabatic and diabatic regions in the quasienergy spectrum can be made for our experiment where the field turn-on is so slow that the initial $n_0\,{}^3S$ state joins adiabatically to the $|q_{S,0}\rangle$ quasienergy state. In Fig. 11 the downward bending $|q_{S,0}\rangle$ energy level is indicated as $(S,10)$ and, equivalently, as $(S,8)$, where the second number between brackets indicates the zero-field (relative) photon number. On the other hand, for the narrow anticrossings encountered by the $|q_{S,0}\rangle$ state (such as shown in Fig. 12), the turn-on of the field is so rapid that they will be traversed diabatically.

As a first approximation to the dynamics generated by the field switching, therefore, we replace in Eq. (20) $|\alpha,0\rangle$ by $|q_{S,0}\rangle$. In other words, at each of the narrow anticrossings such as are shown in Fig. 12 the $|q_{S,0}\rangle$ initial state and $|q_{L,k}\rangle$ final high-L manifold states act as diabatic states whose interaction is switched suddenly. The $|q_{L,k}\rangle$ state is the quasienergy state that joins to the $n_0\,{}^3L$, $L>2$ atomic state at zero field. Retention in Eq. (20) of the state $|\beta,k\rangle$ instead of $|q_{L,k}\rangle$ is equivalent to the assumption that for these high-L, near-degenerate manifold states the field turn-off to zero is sudden.

For the relatively few states contributing to the sum in Eq. (20), the transition probability can be computed efficiently using an inverse iteration technique that is described in Appendix B. Figure 11(a) shows the transition probability $\sum_{l=3}^{n-1}P(n\,{}^3S\rightarrow n\,{}^3l)$ for $n=28$ and with τ in Eq. (20) taken as the cavity traversal time. The summed transition probability is an incoherent sum over those atomic induces β in Eq. (20) that correspond to $L>2$ manifold states. Sharp peaks are predicted precisely (within the experimental accuracy) where the experiment [Fig. 8(a)] shows dips.

2. *The influence of the field envelope*

The above procedure may reproduce the positions and approximate depths of the observed structures, but in order to understand their *shape,* we should realize that our crude distinction between adiabatic and diabatic states must break down when the maximum field strength inside the cavity is set just beyond an anticrossing, such as is shown in Fig. 12. Due to the finite curvature of the field envelope function $A(t)$, that anticrossing will be traversed slowly when the field amplitude rises to its maximum value and again when the field is switched off, slower as the maximum field amplitude is set closer to the anticrossing field. In other words, the coupling between the diabatic states $|q_{S,0}\rangle$ and $|q_{L,k}\rangle$ can no longer be regarded as being switched suddenly. Instead, in a small interval of field amplitudes the anticrossing between both states will be transversed partly diabatically and partly adiabatically.

Figure 13 shows the energy of two interacting quasienergy states (that were taken from Fig. 11) as function of time for two different transient functions $A(t)$. One corresponds to the slower turn-on of cavity *II* (*III*), and the other to the faster turn-on of cavity *IV*. The figure bears a striking resemblance to the situation in an atomic collision. As was pointed out in Sec. I, this resemblance underscores a deep analogy between spectroscopy and collision physics and is based on the presence of two disparate time scales in both cases. In general, an anticrossing is encountered twice, once upon entrance of the cavity and once upon exist. When its traversal is partly adiabatic and partly diabatic, interference between both paths occurs, and the transition probability exhibits oscillations that are known as Stückelberg oscillations in atomic collision theory. In the present situation, when the field amplitude rises (well) above the anticrossing field strength and both anticrossings are well separated in time, the LZS formula, supplemented by an analogous derivation for the phase evolution, suffices to compute the multiphoton transition probability. However, at the other extreme, if the field amplitude is set precisely at the anticrossing field, both anticrossings merge, and the so-called Nikitin exponential model applies.[6] Thus, by scanning the microwave power coupled into the cavity

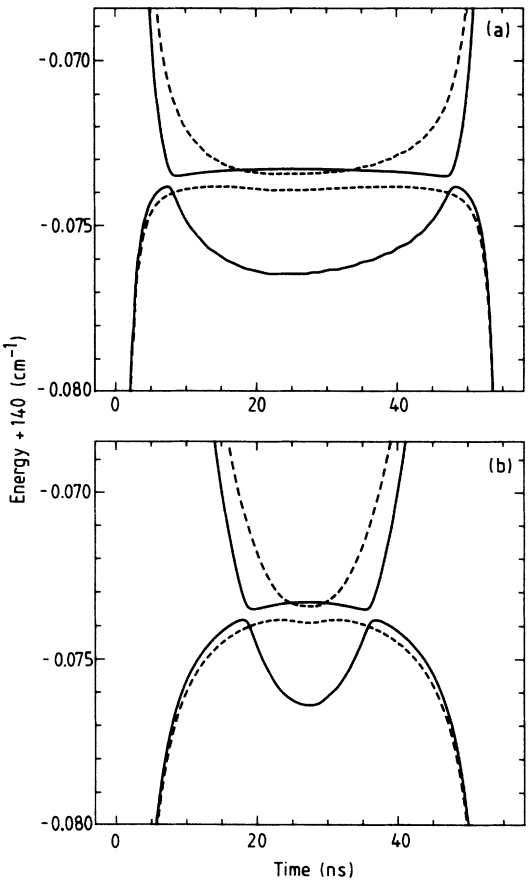

FIG. 13. Time-dependent energy of two quasienergy levels engaged in an anticrossing as a function of time since passage of the cavity entrance. Shown are the states that avoid crossing at 52.9048 V/cm in Fig. 11. (a) With the faster turn-on in cavity *IV*; solid line: maximum field amplitude set at 53.1000 V/cm, dashed line: at 52.9048 V/cm (the anticrossing field). (b) Same as (a) but for cavity *II* (*III*) with the slower turn-on.

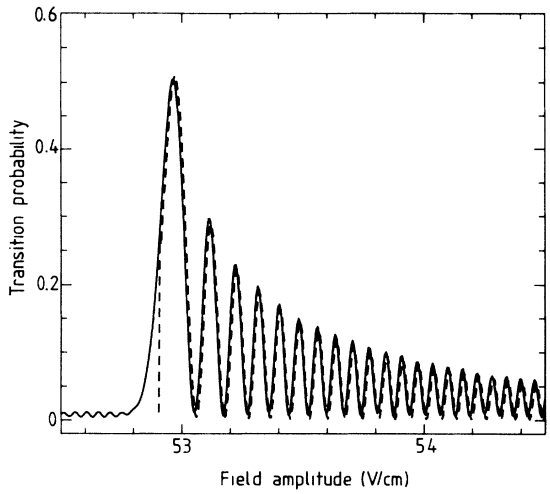

FIG. 14. Probability of transitions between the two interacting quasienergy levels in Fig. 13(b) as a function of maximum field amplitude inside cavity *II* (*III*). Solid line: as computed from numerically integrating the time-dependent Schrödinger equation of a six-state model; dashed line: as computed form the LZS formula.

(Fig. 13 shows two power settings), there is a continuous transition from one type of collisional encounter to the other one.

The transition probability as a function of field amplitude is shown in Fig. 14. It was computed for the same quasi-energy states shown in Fig. 13 and for the transient function $A(t)$ of cavity *II* (*III*). The figure compares the result of a numeric integration of the time-dependent Schrödinger equation [Eq. (8)] with the analytical result from LZS theory. Of course, near the anticrossing field amplitude the analytical result is invalid; however, the discrepancy with the numerical result remains confined to a remarkably narrow field interval.

A closer inspection of the computed Floquet spectrum for $n_0=28$ in Fig. 12 reveals that in the relevant interval of field amplitudes (approximately from 44 until 54 V/cm), the interaction between the initial $|q_{S,0}\rangle$ quasienergy state and the high-L $|q_{L,k}\rangle$ manifold states remains confined to a few well-isolated anticrossings. To a good approximation, the energies of those states also vary linearly with the field amplitude. The situation in the case of $n_0=29$ is quite similar. Each of those respective regions of interest was, therefore, modeled with six diabatic states whose energies varied linearly with the field amplitude. It was also assumed that the only interaction in the model occurred between the state representing the initial $|q_{S,0}\rangle$ quasienergy state and the five remaining $|q_{L,k}\rangle$ "manifold" states. The five corresponding matrix elements were adjusted such as to produce the same anticrossing widths as those in the full Floquet calculation. The $L>2$ component of the model states was determined by equating the amplitude of Rabi oscillations to those computed from Eq. (20) for the full quasienergy spectrum.[38]

These simple but adequate models with time-dependent energies that followed from the amplitude envelope function $A(t)$ enabled the integration of the time-dependent Schrödinger equation [Eq. (8)] for the transient response of the atom to the switched radiation field. (Let us again contrast the use of Eq. (8) made here to that in Sec. IV A, where it was employed to study the response of the atom to the *instantaneous* electric field.) The resulting spectra were averaged over the radial variation of the electric field amplitude in the cavity. To this aim, the spectra were convoluted with the right-hand side of Eq. (1), assuming that the collimator aperture that defined the radial extent of the atomic beam was illuminated uniformly.

Figure 15 shows enlargements of the microwave excitation spectra for $n_0=28,29$ that were measured with two different field switching functions $A(t)$. The computed spectra are also shown in Fig. 15. The calculations predict tails at the high-field side of the dips, tails that are observed in the experiment. Those tails consist of unresolved Stückelberg oscillations. Due to the accumulation of large phase differences in the "bows" of Fig. 13, oscillations in the computed transition probability were so rapid that they remained obscured in the convolution

over the radial variation of the field amplitude. A striking discrepancy is, however, that the theory predicts narrower structures than those observed in the experimental result. Some of the computed dips in Fig. 15(b) are slightly displaced from the measurement; this shift, however, consistent with the quoted (5%) uncertainty of the field calibration.

Experimental broadening effects, other than the radial variation of the field amplitude in the cavity, may provide a partial explanation for the found width discrepancies. Possible candidates are the presence of low-frequency noise in the microwave system or the existence of a small but nonzero angle θ_b between particle trajectories and the cavity axis. An approximate bound on θ_b is given by the beam pencil angle as determined by the beam collimation. It is estimated to be $\theta_b < 0.31°$, giving rise to an extra field broadening of 50% for the dips in Fig. 15(c).

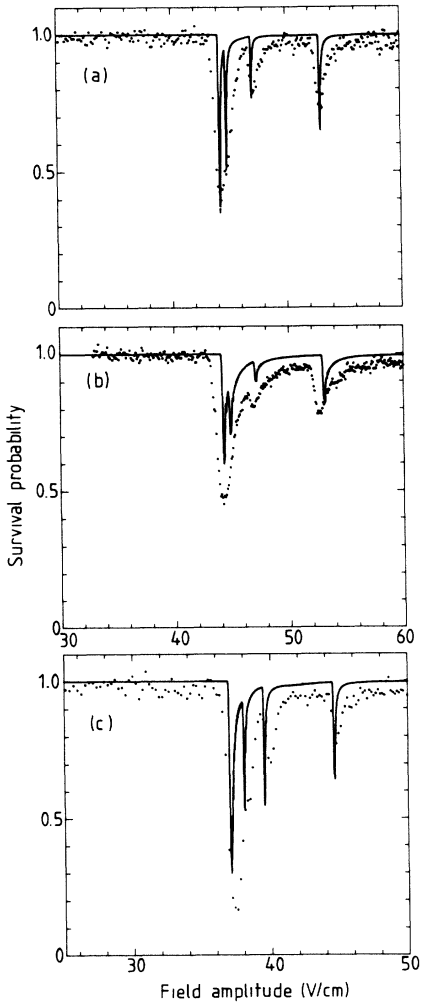

FIG. 15. (a) Dots: measured survival probability of He 28 ^3S atoms as a function of on-axis electric field amplitude in cavity *IV* (the faster cavity). Line: the complement of $n\,^3S \rightarrow n\,^3L > 2$, $n=28$ excitation probability computed from a model of six interacting states and allowing for the field-switching transients. (b) The same as (a) but for the slower cavity (cavity *III*). (c) The same as (a) but for $n=29$.

The magnitude of the combined effect of both broadening mechanisms may also be estimated from the sharpness of the leading edge of the dips, which in case of Fig. 15 extends over approximately 0.6 V/cm. Because both effects are expressed as a convolution over the computed spectra, they will broaden the dips, but at the same time will also reduce their depth. Near the cavity entrance and exit, atoms traveling off axis experience a small, radially directed component of the microwave "fringe" electric field. However, its numerically computed magnitude is always a small fraction ($< 10\%$) of that of the longitudinal component, so we speculate its effect to be negligible.

A fundamentally different source of broadening would be a possible decay of coherence of the microwave field during passage of a single atom. This could be caused by small amplitude or phase fluctuations of the microwave oscillator. To set the scale of the amplitude fluctuations that could cause such a coherence loss, we notice from Fig. 14 that an amplitude change of approximately 0.1 V/cm causes the phase accumulated in the "bows" of Fig. 13 to change by 2π. This amounts to relative amplitude fluctuations of 2×10^{-3}. The noise of the microwave circuit that feeds the cavity is damped by the cavity with a characteristic "ringdown" time $\tau_d = 2Q_0/\omega \cong 3\times10^{-7}$ s, where we have used an unloaded quality factor $Q_0 = 8\times10^3$. Comparison of this time scale to the cavity transit time $\tau \cong 5\times10^{-8}$ s renders this broadening mechanism highly unlikely: the input noise-to-signal ratio would have to exceed unity.

It is obvious that many regions of the quasienergy spectrum cannot be modeled adequately by a few (diabatic) states which interact only locally and pairwise. This will, in particular, be the case when the repulsion between quasienergies, such as is shown in Fig. 11, is strong and three or more states simultaneously interact. An interesting example is the tangle of anticrossings at 70 V/cm, which is precisely at the field strength where in case of $n_0 = 28$, the first broad features emerges in Fig. 8(a). We now show that an understanding of the dynamics of anticrossing transversal is crucial for understanding the position and shape of this observed structure. Figure 16(b) shows an enlargement of the relevant portion of the quasi-energy spectrum together with our attempt [frame (c)] to model it with only seven diabatic states. Frame (a) also shows the predicted shape of the microwave quench measurement together with the experimental result. The energies of the model states and their pairwise matrix elements were determined by fitting the model to the full quasienergy spectrum shown in frame (b).

The model calculation does approximately reproduce the shape of the observed broad dip and also predicts that its minimum (at 68 V/cm) is located beyond the field amplitude where the wide anticrossing occurs (at 65.5 V/cm).[39] This is a direct consequence of the dynamics of anticrossing traversal which is predominantly adiabatic until the maximum field amplitude inside the cavity is set to about 68 V/cm. An important discrepancy between the model spectrum and the result of the experiments is, however, that the former shows much more structure than is experimentally observed. This discrepancy may in part be explained by obvious deficiencies in the adia-

batic model used to represent the Floquet spectrum.[40] We emphasize, however, that this result clearly illustrates the influence of the switching dynamics on the shape of multiphoton resonances.

V. CONCLUSION

Several years ago, Zimmerman *et al.* designed simple but practical tools that provided guidance in spectroscopy of Rydberg atoms in static electric fields.[16] However, since these tools were of a fundamentally perturbative nature, a different approach was needed for a full theory that could also encompass the essential continuum character of the problem.[21] This approach was found and developed to allow precise reconstruction of the Stark spectrum using only a few parabolic channels among which the interaction was expressed directly in the parameters of the atomic structure, namely the quantum defects.

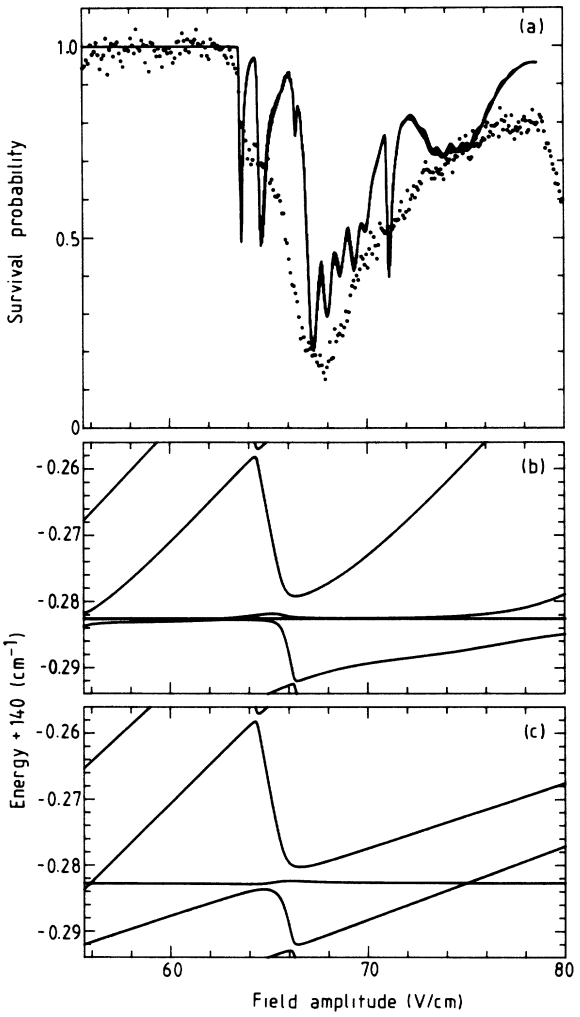

FIG. 16. (a) Dots: enlargement of $n=28$ microwave quench spectrum shown in Fig. 8(a). Line: spectrum computed from integration of the time-dependent Schrödinger equation using a model of seven diabatic states and fitted pairwise interaction matrix elements. (b) Quasienergy spectrum from a full Floquet diagonalization (see Fig. 11). (c) Quasienergy spectrum computed from the seven-state model.

In the present article we faced a similar situation: Elementary Floquet theory allows a precise reproduction of the position of observed features in excitation curves obtained with microwave electric fields. However, in order to understand their shape, we had to resort to a crude modeling of the spectrum. So far, we have found no simple way to extract directly the relevant information from the known zero-field atomic structure (i.e., the quantum defects). Neither have we yet found a simple way to extract these parameters from the Floquet calculation. We anticipate, therefore, that a more satisfying theory for the ac Stark problem will have to be formulated on a different basis, much as in the case of the dc Stark problem.

The first step towards this goal may be to retain only the largest ($L=0$) quantum defect in the Floquet diagonalization. It may well be that such an approximation reproduces the gross structure of the quasienergy spectrum, and that the size of the small avoided crossings that are responsible for the effects studied in this paper scales with the higher-L quantum defects. Another promising approach to a more systematic construction of diabatic models may be provided by the so-called generalized Van Vleck nearly degenerate perturbation method.[41]

It should be realized, however, that we are not bound to models based upon *diabatic* states. A strictly equivalent approach would start from the complementary *adiabatic* basis. Although this would lead to more involved numerics, all necessary ingredients can now be extracted from the Floquet diagonalization. Still, also the adiabatic approach bypasses what we feel is the main problem here, namely that the parameters of the atomic structure seem to entangled in a very complex manner in the quasienergy spectrum. We hope that a future theory will succeed in unraveling this tangle.

ACKNOWLEDGMENTS

The authors are deeply indebted to Dr. Tom Bergeman, who started the Floquet calculation described in this paper. They also thank Dr. H. Kirk for making available computing facilities at the Center for Accelerator Physics at Brookhaven National Laboratory. The work at Eindhoven was supported by the Netherlands Organization for Scientific Research (NWO); that at Stony brook was supported by the Atomic, Molecular and Plasma Physics Program of the U.S. National Science Foundation.

APPENDIX A: CORE-INTERACTION MATRIX ELEMENTS

In this section we propose a slight alteration of Eqs. (10) and (11) that allowed us to compute core-interaction matrix elements between parabolic states. The restriction of the parabolic basis set to a few, say N, manifolds may be viewed as a projection, with the associated projection operator P being defined as

$$P|\Psi\rangle = \sum_{j\,(<N)} S_{ij}|\phi_j\rangle \ , \tag{A1}$$

with $S_{ij}=\langle\psi_i|\phi_j\rangle$, where $|\psi_i\rangle$ is a zero-field He wave function with energy $\tilde{\varepsilon}_i=-1/2(n_i-\mu_{l_i})^2$ and $|\phi_j\rangle$ a H wave function with energy $\varepsilon_j=-1/2n^2$. The P-projected He wave function at the same energy as the exact wave function satisfies

$$(PH_0P+\tilde{V})P|\psi_i\rangle=\tilde{\varepsilon}_iP|\psi_i\rangle\ , \tag{A2}$$

where the core interaction is replaced by an optical potential $\tilde{V}$. We approximated its matrix elements by

$$\tilde{V}_{kl}=\langle\phi_k|\tilde{V}|\phi_l\rangle=\sum_{i\,(<N)}S_{ik}(S^{-1})_{il}\tilde{\varepsilon}_i-\varepsilon_k\delta_{kl}\ , \tag{A3}$$

where $(S^{-1})_{ij}$ are the elements of the inverse of S; $i,j<N$. An approximate analytical expression for the elements of S can be derived using the basis functions of quantum-defect theory[42]

$$S_{ij}\cong\frac{\sin(\pi\mu_l)}{\pi}(-1)^{n_i+n_j}\times\frac{(B_i/B_j)^{1/2}}{[1/2(n_i-\mu_l)^2-1/2n_j^2][(n_i-\mu_l)n_j]^{3/2}}\ , \tag{A4}$$

with the products $B_l=\prod_{p=0}^{l}(1-p^2/2n_l^2)$ differing only slightly from 1. Using Eqs. (A3) and (A4) for two interacting manifolds, we retrieve the result of Komarov, Grozdanov, and Janev in the limit of vanishing quantum defects.[28] From Eq. (A3) it is also clear that the optical potential is non-Hermitian. In order to be able to use conservation of probability as a check of the numeric integration, we therefore symmetrized the interaction matrix by replacing $\tilde{V}_{kl}$ with $(\tilde{V}_{kl}+\tilde{V}_{lk})/2$.

As may be judged from Fig. 10, the approach that starts from parabolic states with the above sketched approximation of their core-induced interaction is clearly inferior to a description based on zero-field spherical states that was used in the Floquet diagonalization. In Fig. 10 the first three multiphoton resonances are predicted at field amplitudes that are almost 3 V/cm below those observed experimentally.

APPENDIX B: COMPUTING TRANSITION PROBABILITIES

In this section we discuss a partially graphical method for the computation of the right-hand side of Eq. (20)

$$P_{\beta\leftarrow\alpha}(\tau)=\sum_{\substack{\gamma,m\\ \gamma',m'}}\langle\beta,k|q_{\gamma,m}\rangle\langle q_{\gamma,m}|q_{S,0}\rangle\langle q_{S,0}|q_{\gamma',m'}\rangle\times\langle q_{\gamma',m'}|\beta,k\rangle e^{i(q_{\gamma m}-q_{\gamma' m'})\tau}\ , \tag{B1}$$

where we have dropped the summation over the photon number k of the final state. This is justified because the coupled $|q_{\gamma,m}\rangle$ and $|q_{\gamma',m'}\rangle$ states have simultaneous overlap with the initial state $|q_{S,0}\rangle$ and only a single $|\beta,k\rangle$. The neighboring $|\beta,k-2\rangle$ and $|\beta,k+2\rangle$ are too distant in energy compared to the level separation at anticrossings.

As was already emphasized in Sec. IV B 1, the number of terms that contribute to the right-hand side of Eq. (B1) is very small. Namely, the only states $|q_{\gamma,m}\rangle$ that contribute are those that far from an anticrossing have either the character of $|q_{S,0}\rangle$ or $|\beta,k\rangle$. Practically, out of the 700 basis states of Fig. 11, a maximum of only 10 at any field point is needed for the computation of the transition probability. Technically, the Floquet matrix is a symmetric band matrix and needs only a modest amount of computer memory for storage. Finding its eigenvalues is always faster and more convenient than finding and storing the accompanying spectrum of eigenvectors.

We have built a graphical interface to our programs which allows an economical computation of transition probabilities. Our followed procedure was to diagonalize

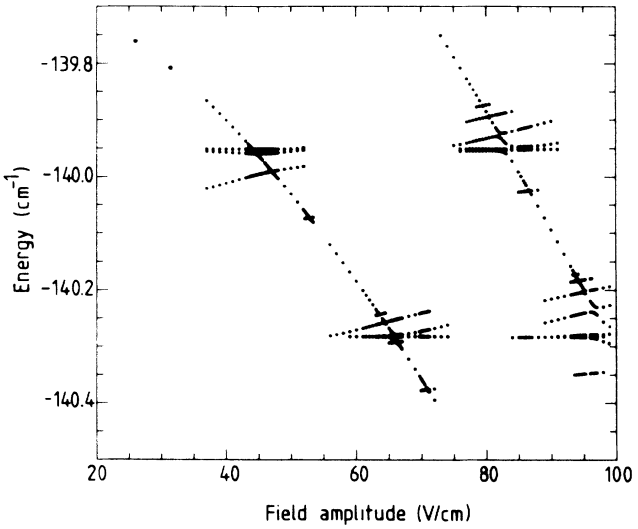

FIG. 17. Graph of a list of Floquet energies extracted from Fig. 11, showing the initial $|q_{S,0}\rangle$ quasienergy state and all other states that are encountered in anticrossings. The list is used as input for calculation of transition probabilities.

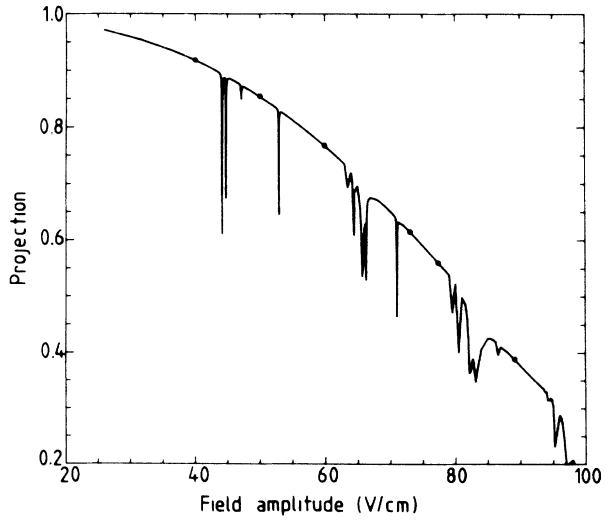

FIG. 18. Full line: maximum $|28\,^3S,0\rangle$ component of states whose energies are shown in Fig. 17. Dots: field strengths used to interpolate the adiabatic initial state $|q_{S,0}\rangle$ through anticrossings.

the Floquet matrix on a course grid of points, which was subsequently refined near anticrossings. Next, the energy of the $|q_{S,0}\rangle$ state was diabatically followed starting from the zero-field $|S,0\rangle$ state. At each encounter of an anticrossing, the energies of the states involved were registered over a field interval that amply embraced the anticrossing. Figure 17 shows a graph of the resulting list of eigenvalues. Because of the periodicity of the Floquet Hamiltonian, the two branches shown actually belong to the same initial adiabatic state $|q_{S,0}\rangle$. Using this list, the corresponding eigenvectors can be found by inverse iteration.

From Figs. 11 and 17 it is clear that the energy of the adiabatic $|q_{S,0}\rangle$ can be smoothly interpolated through the regions of anticrossings. The same is true for the corresponding eigenvector, which outside the narrow regions of anticrossing has predominantly $|S,0\rangle$ character. This is suggestively illustrated in Fig. 18 where the maximum absolute value of the $|S,0\rangle$ component of all eigenvectors corresponding to the list shown in Fig. 17 is plotted. For field amplitudes up to 80 V/cm and away from anticrossings, this maximum is found in the vector $|q_{S,0}\rangle$. At the sharply defined anticrossings the $|q_{S,0}\rangle$ is mixed with other states and loses its otherwise predominantly $|S,0\rangle$ character. In the computation the $|q_{S,0}\rangle$ state vector is then sought at a few field amplitudes far from anticrossings, and is linearly interpolated in between; those field amplitudes are also shown in Fig. 18.

In summary, our graphical method allows the isolation of the adiabatic initial state and the construction of a list of the relevant interacting states that constitute the sum in the right-hand side of Eq. (B1). For the cases analyzed here ($n \simeq 30$) this can be achieved readily with modest computational resources. Our method could, therefore, be employed as a tool for "*quasienergy spectroscopy*."

[1]E. J. Galvez, B. E. Sauer, L. Moorman, P. M. Koch, and D. Richards, Phys. Rev. Lett. **61**, 2011 (1988); J. E. Bayfield, G. Casati, I. Guarneri, and D. W. Sokol, *ibid.* **63**, 364 (1989); P. M. Koch, L. Moorman, B. E. Sauer, E. J. Galvez, K. A. H. van Leeuwen, and D. Richards, Phys. Scr. **T26**, 51 (1989), and references therein.

[2]D. Richards, J. G. Leopold, P. M. Koch, E. J. Galvez, K. A. H. van Leeuwen, L. Moorman, B. E. Sauer, and R. V. Jensen, J. Phys. B **22**, 1307 (1989).

[3]L. I. Schiff, *Quantum Mechanics* (McGraw-Hill, New York, 1968), p. 234.

[4]P. Pillet, W. W. Smith, R. Kachru, N. H. Tran, and T. F. Gallagher, Phys. Rev. Lett. **50**, 1042 (1983).

[5]D. R. Mariani, W. van de Water, P. M. Koch, and T. Bergeman, Phys. Rev. Lett. **50**, 1261 (1983); see also P. M. Koch, J. Phys. (Paris) Colloq. **43**, C2-187 (1982).

[6]E. E. Nikitin and S. Ya Umanski, *Theory of Slow Atomic Collisions* (Springer, Berlin, 1984).

[7]W. S. Warren, Science **242**, 878 (1988).

[8]H. P. Breuer, K. Dietz, and M. Holthaus, Z. Phys. D **8**, 349 (1988); **10** 13 (1988).

[9]A. Szöke, in *Atomic and Molecular Processes with Short Pulses,* edited by A. D. Bandrauk (Plenum, New York, 1988), p. 207.

[10]H. G. Muller, H. B. van Linden van den Heuvell, P. Agostini, A. Antonetti, M. Franco, and A. Migus, Phys. Rev. Lett. **60**, 565 (1988).

[11]R. C. Stoneman, D. S. Thomson, and T. F. Gallagher, Phys. Rev. A **37**, 1527 (1988). The results of earlier experiments on microwave multiphoton transitions that were tuned into resonance by an external static electric field were reported by L. A. Bloomfield, R. C. Stoneman, and T. F. Gallagher, Phys. Rev. Lett. **20**, 2512 (1986).

[12]U. Eichmann, J. L. Dexter, E. Y. Xu, and T. F. Gallagher, Z. Phys. D **11**, 187 (1989).

[13]The explanation given by Stoneman and co-workers (Ref. 11) leaves many questions that will be raised in S. Yoakum, W. van de Water, L. Moorman, K. A. H. van Leeuwen, and P. M. Koch (unpublished). These questions mainly concern an explanation for the large width of the structure observed in potassium. This width is contrasted with the results of a Floquet analysis of the 9.278-GHz microwave excitation of the K(19*S*) state that predicts a series of very narrow peaks.

[14]J. Singh, X. Sun, and K. B. MacAdam, Phys. Rev. Lett. **58**, 2201 (1987).

[15]W. van de Water, D. R. Marini, and P. M. Koch, Phys. Rev. A **30**, 2399 (1984).

[16]M. L. Zimmerman, M. G. Littman, M. M. Kash, and D. Kleppner, Phys. Rev. A **20**, 2251 (1979).

[17]K. Halbach and R. F. Holsinger, Part. Accel. **7**, 213 (1976).

[18]B. E. Sauer, K. A. H. van Leeuwen, A. Mortazawi-M., and P. M. Koch (unpublished). The mode volume πLR^2 in Eq. (2) needs correction due to the cavity entrance and exit apertures. This correction was, however, numerically found to be completely negligible.

[19]In the vicinity of the endcap holes there was both a static electric field (from the label potential) and a microwave electric field, both varying spatially. Therefore atoms traveling on different trajectories experienced somewhat different combined static and microwave fringe fields. We presume that the occasionally observed variations in details of measured ionization curves were due to these slight variations in combined fields.

[20]R. J. Damburg and V. V. Kolosov, J. Phys. B **12**, 2637 (1979), and references therein; and in *Rydberg States of Atoms and Molecules,* edited by R. F. Stebbings and F. B. Dunning (Cambridge University Press, New York, 1983).

[21]D. A. Harmin, Phys. Rev. A **30**, 2413 (1984).

[22]L. D. Landau, Phys. Z. Sowjetunion **2**, 46 (1932); C. Zener, Proc. R. Soc. London Ser. A **137**, 696 (1932); E. C. G. Stückelberg, Helv. Phys. Acta **5**, 369 (1932).

[23]D. R. Bates, Proc. R. Soc. London Ser. A **257**, 22 (1960).

[24]In a sinusoidally varying field the lower and upper bounds of the transition region would be given by $F_{l,u} = F_0 \sin(\omega\tau_{l,u} + \varphi)$, where $\tau_{l,u}$ is the appropriate solution branch off

$$(d\Delta E/dF)F_0 \int_0^{\tau} [\sin(\omega t + \varphi) - \sin(\varphi)]dt = \frac{\pi s}{2} ,$$

and $F_c = F_0 \sin(\varphi)$ is the crossing field. Substituting the same, typical values ($F_c = 130$ V/cm, $\omega/2\pi = 9.9$ GHz) in this equation teaches that for $F_0 \geq F_c$ the lower bound of the transition region trails about 40 V/cm behind the maximum field strength F_0. The upper bound equals F_0 for $F_0 \leq 156$ V/cm, where the phase difference built up between the instant the anticrossing is passed and the moment at which the instantaneous field reaches its maximum falls short of $\pi s/2$. For larger field amplitudes F_0 the upper bound $F_u \leq F_0$ and asymptotically approaches that given in Eq. (3). The statement based on Eq. (3) should therefore be refined in the sense that only the first anticrossing met when F_0 is increased could give rise to two-state dynamics. Such two-state dynamics would, of course, also require that the core interaction induces only pairwise interactions among parabolic states. The fact that transitions are not localized, however, remains also in the case of a sinusoidally varying field.

[25]M. J. Seaton, Proc. Phys. Soc. London **88**, 815 (1966). For the quantum defects of higher-angular-momentum states ($L > 3$) we used a polarization formula, with core polarizability 0.281 25.

[26]All standard routines used were provided by the NAG, Numerical Algorithms Group, Oxford, United Kingdom.

[27]L. D. Landau and E. M. Lifshitz, *Quantum Mechanics (Non-Relativistic Theory)*, 3rd ed. (Pergamon, Oxford, 1976), Secs. 36 and 37.

[28]I. V. Komarov, T. P. Grozdanov, and R. K. Janev, J. Phys. B **13**, L573 (1980).

[29]J. H. Shirley, Phys. Rev. **138**, B979 (1965).

[30]A. Maquet, Shih-I Chu, and W. P. Reinhardt, Phys. Rev. A **27**, 2946 (1983).

[31]D. R. Bates and A. Damgaard, Philos. Trans. R. Soc. London **242**, 101 (1949).

[32]As was pointed out in a slightly different context by H. P. Breuer and M. Holthaus, Z. Phys. D **11**, 1 (1989), convergence problems are most evident near anticrossings. Another check on convergence is the degree of periodicity of the numerically computed spectrum. In our case ($n = 28$ with 25 photon bands, $n = 29$ with 31 photon bands), periodicity of the central two bands was to within 2×10^{-6} cm^{-1} for field amplitudes $F_0 < 80$ V/cm. Of course, at the highest field strengths, atomic states of the neighboring manifolds should be included with an accompanying increase of the number of photon states to at least 40.

[33]H. B. van Linden van den Heuvell, R. Kachru, N. H. Tran, and T. F. Gallagher, Phys. Rev. Lett. **53**, 1901 (1984).

[34]M. Abramowitz and I. A. Stegun, *Handbook of Mathematical Functions* (Dover, New York, 1972), p. 366.

[35]K. F. Milfield and R. E. Wyatt, Phys. Rev. A **27**, 72 (1983). Note that this manner of Floquet analysis produces all quasienergies modulo $\hbar\omega$. This circumstance makes quasienergy graphs difficult to interpret.

[36]See J. Shirley, Ref. 29, p. 985; R. Blümel and U. Smilansky, Z. Phys. D **6**, 83 (1987), have linked the appearance of structure in hydrogen microwave ionization curves with the occurrence of unresolved clusters of (many) anticrossings between quasienergy levels.

[37]See, for example, M. H. Mittleman, *Theory of Laser-Atom Interactions* (Plenum, New York, 1982), Chap. 2.

[38]This procedure assumed that the $L > 2$ "manifold" quasienergy states are projected on the corresponding bare atomic states when the field is switched off. Adapating an adiabatic connection instead would, for example, increase the depth of the smallest dips in Fig. 15(a) by approximately 30%. The field-switching-induced dynamics of almost degenerate high-L manifold quasienergy states remains a topic of future investigation.

[39]Although the difference betwen 68 and 65.5 V/cm falls within the quoted 5% uncertainty in the field calibration, the position of two other predicted sharp features correlates well within this uncertainty with that of features that can be observed at 64 and 71.5 V/cm in the experimental curve.

[40]In our assumption of a model of diabatic states we have also neglected phases associated with the second term in the left-hand side of Eq. (6). In the case of field variations in more than one dimension this term gives rise to the so-called Berry phase: M. V. Berry, Proc. R. Soc. London Ser. A **392**, 45 (1984).

[41]T. S. Ho, C. Laughlin, and S. I. Chu, Phys. Rev. A **32**, 122 (1985), and references therein.

[42]M. J. Seaton, Rep. Prog. Phys. **46**, 167 (1983).